96-73

Environment Canada

Water Science and Technology Directorate

Direction générale des sciences et de la technologie, eau

Environnement Canada

Sulfide Mineral Oxidation and Subsequent Transport of Oxidation Products in Mine Tailings Impoundments: A Numerical Model

By:

Wunderly, M., Blowes, D.W., Frind, E.O., Ptacek, C.J.

TD
226
N87
No. 96-
73

96-73

Title: Wunderly, M., Blowes, D.W., Frind, E.O., **Ptacek, C.J.** Sulfide mineral oxidation and subsequent transport of oxidation products in mine tailings impoundments: A numerical model. Submitted to Water Resources Research (revised January, 1996), 46 pp.

Management Perspective: We have developed a new model to describe sulfide mineral oxidation and the subsequent transport of oxidation products in mine tailings. A shrinking-core model is used to represent sulfide-mineral oxidation in the unsaturated zone, and a steady-state reactive solute transport model is used to represent transport of the oxidation products in the unsaturated and saturated zones. The reactive solute transport model includes many dissolved species and reaction types, including precipitation and dissolution reactions, and adsorption reactions. The model can be used to simulate pyrite or pyrrhotite oxidation under spatially variable moisture contents, and the subsequent transport of the oxidation products in variable tailings types. It can also be used to evaluate the potential benefits of remediation and design alternatives.

Abstract: A versatile numerical model that couples oxygen diffusion and sulfide-mineral oxidation (PYROX) has been developed to simulate the oxidation of pyrite in the vadose zone of mine tailings. A shrinking-core oxidation model and a finite element numerical scheme are used to simulate the transport of oxygen and oxidation of pyrite grains. The rate of pyrite oxidation is assumed to be limited by the transport of oxygen to the reaction site. The model determines the spatially variable bulk diffusion coefficient for oxygen based on moisture content, porosity, and temperature, all of which are variable input parameters. The model PYROX has been coupled to an existing reactive transport model (MINTRAN), which uses a finite element scheme for transport of contaminants, and MINTEQA2 to solve for the equilibrium geochemistry. The reactions described by MINTRAN are subject to the local equilibrium assumption. The resulting model, MINTOX, is capable of simulating tailings impoundments where the oxidation of pyrite or pyrrhotite is causing acidic drainage and where acid neutralization and attenuation of dissolved metals can be attributed to equilibrium reactions. Because MINTOX uses realistic boundary conditions and hydrogeological properties, the potential benefits of various remediation schemes, such as moisture-retaining covers, can be quantitatively evaluated.

SULFIDE MINERAL OXIDATION AND SUBSEQUENT REACTIVE TRANSPORT OF OXIDATION PRODUCTS IN MINE TAILINGS IMPOUNDMENTS: A NUMERICAL MODEL

M.D. Wunderly[1,2], D.W. Blowes[1], E.O. Frind[1], C.J. Ptacek[1,3]

1. Waterloo Centre for Groundwater Research, University of Waterloo, Waterloo, ON, CANADA
2. *Present Address:* Ogden Environmental and Energy Services Co., Inc., San Diego, CA, USA
3. National Water Research Institute, Environment Canada, Burlington, ON, CANADA

Submitted to Water Resources Research (Revised January 1996)

Abstract. A versatile numerical model that couples oxygen diffusion and sulfide-mineral oxidation (PYROX) has been developed to simulate the oxidation of pyrite in the vadose zone of mine tailings. A shrinking-core oxidation model and a finite element numerical scheme are used to simulate the transport of oxygen and oxidation of pyrite grains. The rate of pyrite oxidation is assumed to be limited by the transport of oxygen to the reaction site. The model determines the spatially variable bulk diffusion coefficient for oxygen based on moisture content, porosity, and temperature, all of which are variable input parameters. The model PYROX has been coupled to an existing reactive transport model (MINTRAN), which uses a finite element scheme for transport of contaminants, and MINTEQA2 to solve for the equilibrium geochemistry. The reactions described by MINTRAN are subject to the local equilibrium assumption. The resulting model, MINTOX, is capable of simulating tailings impoundments where the oxidation of pyrite or pyrrhotite is causing acidic drainage and where acid neutralization and attenuation of dissolved metals can be attributed to equilibrium reactions. Because MINTOX uses realistic boundary conditions and hydrogeological properties, the potential benefits of various remediation schemes, such as moisture-retaining covers, can be quantitatively evaluated.

INTRODUCTION

Mathematical models have been widely used to model chemical and physical hydrogeological phenomena for several decades. As the processing power of computers has increased, so has the sophistication of these models. The finite element method is a robust approach for modelling flow and transport, while geochemical equilibrium codes have been very successful at modelling inorganic chemistry. However, there are relatively few models that take into account both the physical transport and equilibrium chemistry, and even fewer that consider kinetically controlled chemical reactions. The mine-tailings environment exhibits extreme geochemical variations, some of which can be modelled using an equilibrium approach; others require a kinetic approach.

Various geochemical reactions take place within mine tailings including sulfide-mineral oxidation, redox, aqueous speciation, acid-base, mineral precipitation/dissolution, and ion exchange reactions. When the physical transport of chemicals within the tailings is slow compared with the rate at which the chemical reactions occur, the local equilibrium assumption (LEA) is reasonable, and an equilibrium approach to reactive transport modelling may be used. This approach assumes that all chemical species are in thermodynamic equilibrium. However, if the reaction rates are slow relative to the rate of physical transport, a kinetic approach should be adopted. An example in which the LEA assumption fails is in the oxidation of pyrite and other sulfide minerals in mine tailings. These reactions may be rate limited by oxygen diffusion into the tailings and may not reach equilibrium for decades or longer.

In general, the solution of equilibrium reactive multicomponent transport is dependent on two sets of equations: the first is the partial differential equations relating to mass transport, and the second is a set of nonlinear algebraic equations relating to the equilibrium chemistry (Yeh and Tripathi, 1989). If any of the reactions involved are kinetically controlled, then additional or modified expressions are required.

Models that simulate equilibrium or kinetically controlled reactive transport generally attempt to solve the problem using either a one- or two-step approach. Direct or one-step equilibrium models

incorporate the chemical equilibrium equations directly into the transport equations. Examples of one-step methods include the models of Rubin and James (1973), Valocchi et al. (1981), Jennings et al. (1982), Miller and Benson (1983), Lichtner (1985), Carnahan (1990), and Steefel and Lasaga (1990).

Two-step equilibrium models divide the solution into two separate parts: advective-dispersive transport and chemical equilibrium. These separate parts are then linked together using various methods.

One-step kinetic models incorporate the reaction rate equations directly into the transport equations similar to one-step equilibrium models. One-step kinetic models include Molz et al. (1986), MacQuarrie et al. (1990), MacQuarrie and Sudicky (1990), and Frind et al. (1990). Two-step kinetic models divide the solution into an advective-dispersive part and a chemical part similar to the two-step equilibrium approach. Two-step examples of kinetic models include Borden and Bedient (1986), Kinzelbach et al. (1991), and Zysset et al. (1994a,b).

The oxidation of pyrite and other sulfide minerals in mine tailings is responsible for the high acidity and mobility of heavy metals observed. In many cases, the rate of oxidation of these minerals is limited by the rate at which oxygen from the impoundment surface can diffuse into the tailings (Davis and Ritchie, 1986; Elberling et al., 1994). As individual particles within the tailings oxidize, a coating of oxidized material forms around an unoxidized core. This oxidized coating acts to further inhibit oxygen from reaching the reaction site. Several models have been proposed to describe the sulfide-mineral oxidation process.

Cathles (1979) examined the predictive capabilities of a finite difference model for copper leaching that includes air convection, heat balance, temperature-dependent mixed oxidation kinetics, and bacterial catalysis. Jaynes et al. (1984a,b) presented a variation of the model described by Cathles and Apps (1975). Their model considers diffusion of oxygen into the pore space to be the main mechanism of oxygen transport. Also included in their model are reaction kinetics, oxygen and ferric iron oxidation of pyrite, bacterial catalysis, complexation and precipitation of ferric iron, and reactions between the hydrogen ions in solution and the solid matrix of the waste. For conditions that would be expected to

exist at reclaimed tailing sites, they found the oxygen diffusion rate is the primary factor in controlling the rate of pyrite oxidation.

Davis and Ritchie (1986) developed a mathematical model for pyrite oxidation in waste rock dumps where diffusion of oxygen to the reaction sites is the rate-limiting factor. The model uses a two-stage approach: first, the diffusion of oxygen into the pore space of the tailings, and second, a shrinking core model to describe the diffusion of oxygen into the individual particles through the oxidized coating that forms around the unreacted core of the particles (Figure 1). Their model is widely accepted and used. Pantelis and Ritchie (1991) developed a model that includes convection and diffusion as transport mechanisms for oxygen within waste rock dumps. They found that for waste rock permeabilities of less than 10^{-10} m^2, convection of oxygen is not a significant mechanism of oxygen transport for several years. Because the permeabilities of mine tailings are considerably lower than those of waste rock, it is unlikely that convection of oxygen is an important mechanism for oxygen transport in mine-tailings environments. Jaynes et al. (1984b) found that the interaction between H^+ produced during the oxidation of pyrite and the tailings solids is crucial in determining the pH of the tailings water. A model has not yet been developed that adequately deals with pyrite oxidation and the subsequent reactive transport of the oxidation by-products, namely H^+, Fe(II), Fe(III), and SO_4^{2-}.

The first objective of this study was to develop an oxygen diffusion and pyrite oxidation model for nonhomogeneous media. The model (PYROX) considers pyrite to be the only sulfide mineral undergoing oxidation. A modification of the model permits the selection of pyrrhotite as the only sulfide mineral. Other sulfide minerals will be considered in future work. PYROX assumes the oxidation of pyrite to be rate limited by the physical transport of oxygen to the reaction site. This assumption ignores the role of bacteria and reaction kinetics by assuming that the rate at which pyrite oxidizes is fast relative to the oxygen diffusion rate. The conceptual and mathematical development of PYROX was based on the work of Davis and Ritchie (1986), which in turn was based on the mathematical development of Levenspiel (1972).

The second objective of this study was to couple PYROX to an existing reactive transport code, MINTRAN (Walter et al., 1994a,b). The resulting model, MINTOX, calculates masses of reaction products produced by the oxidation of pyrite and the subsequent reactive transport of these reaction products. The reactions described by MINTRAN are subject to the local equilibrium assumption. Therefore, geochemical systems where equilibrium is not achieved during each time step will not be modelled accurately using this approach.

MATHEMATICAL MODEL DEVELOPMENT FOR OXYGEN DIFFUSION AND PYRITE OXIDATION (PYROX)

In many cases, the diffusion of oxygen into mine-tailings impoundments can be considered a one-dimensional (1-D) problem. This assumption is reasonable because mine tailings are commonly spread laterally over hundreds or thousands of square meters, whereas the depth over which oxidation occurs is commonly only a few meters. The direction of oxygen diffusion is generally from the surface downward to the water table. At the impoundment surface, the concentration of oxygen is constant and equal to the atmospheric concentration of oxygen (first-type boundary condition). The water table constitutes a zero concentration gradient (second-type) boundary condition. Tailings impoundments of irregular shapes or with high dams may require a two-dimensional model.

The numerical model developed describes oxygen diffusion and pyrite oxidation similar to that presented by Davis and Ritchie (1986), except that several of the variables are dimensioned rather than dimensionless quantities. This form is necessary for compatibility with MINTRAN and to accommodate the spatially variable character of sulfide-mineral content, porosity, bulk density, and moisture content. The resulting equations are very similar to those developed by Davis (1983), and Davis and Ritchie (1986); thus, the same algorithm was used to solve them. Because of its versatile nature, the Galerkin finite element method was chosen to solve the diffusion part of the problem.

BULK DIFFUSION INTO TAILINGS

The mass-balance equation governing bulk diffusion into the pore space of the tailings can be written mathematically as

$$apor(x)\frac{\partial U_A^*(x,t)}{\partial t} = D1(x)\frac{\partial^2 U_A^*(x,t)}{\partial x^2} - q(x,t) \qquad (1)$$

where *apor(x)* is the air-filled porosity of the tailings [m^3/m^3], *D1(x)* is the diffusion coefficient for the porous media [m^2/s], U_A^* is the oxygen concentration in the pore space [kg/m^3] (* means the variable is dimensioned), *q(x,t)* is the sink term due to oxygen consumption by the particles in the bulk tailings [kg/m^3s]. The diffusion coefficient (D1(x)) is variable in space and is calculated using an empirical expression developed by Reardon and Moddle (1985) based on moisture content, porosity, and temperature for all nodes within the tailings.

$$D1(x) = 3.98\times10^{-9} \times \left[\frac{apor(i) - 0.05}{0.95}\right]^{1.7} \times (Temp)^{1.5} \qquad (2)$$

where the Temperature is in Kelvin.

DIFFUSION OF OXYGEN IN PYRITE PARTICLES

The model assumes that the particles are spherical, uniformly sized, and surrounded by an immobile water film. Particles may be saturated with water; however, this water is considered immobile. Particles that undergo oxidation are assumed to have a homogeneous distribution of pyrite within them. The presence of nonoxidizing particles such as sand will not pose a problem provided they are the same size and shape as the oxidizing particles. All oxidation reactions are assumed to occur in the aqueous phase in contact with or near a reacting solid.

Oxygen in the pore space partitions according to Henry's Law from the gas phase to the aqueous phase of the immobile water film. The oxygen diffuses from the particle surface through the porous oxidized coating toward the unoxidized core of the particle, where the oxidation of pyrite occurs. The diffusion of oxygen into the particles is driven by the oxygen concentration gradient between the surface and the core of the particles (Figure 2). As the reaction between oxygen and sulfide minerals within the particles progresses, the radius of the unreacted core will decrease, while the thickness of the oxidized

shell increases. The rate at which the unreacted core shrinks is about 1,000 times slower than the flow rate of oxygen within the particle; about the same as the density difference between gas and solid (Levenspiel, 1972). It can be assumed, therefore, that the reaction front is stationary with respect to the oxygen concentration gradient between the outside of the particle and the reaction front. Thus, the concentration of oxygen within the oxidized coating of the particles decreases linearly from the outside of the particle surface to the unreacted core boundary (steady-state within one time step). This pseudo steady-state assumption allows simplifications in the development of the sink term in equation 1.

An expression similar to the following for the rate at which oxygen mass diffuses into a single oxidizing particle with a shrinking core was derived by Levenspiel (1972).

$$q_s(x,t) = \frac{d(\text{mass } O_2)}{dt} = 4\pi\, D2\left(\frac{R^* r_c^*(x)}{R^* - r_c^*(x)}\right) U_w^*(x,t) \qquad (3)$$

Where U^*_W is the concentration of oxygen in the water surrounding the particle [kg/m^3], R^* is the unreacted radius of the particle [m], $r_c^*(x)$ is the radius of the reaction front within the particle or the radius of the unreacted core [m], and D2 is the diffusion coefficient for the oxidized rim of the particle [m^2/s].

In mine tailings, the behaviour at the macro scale or representative elementary volume (REV) scale is of interest rather than the behaviour of a single particle. Assuming that the grains within the tailings are perfectly spherical, then the number of particles in a unit volume of tailings can be calculated as

$$\#\text{ particles} = \frac{3(1-\text{por}(x))}{4\pi R^{*3}} \qquad (4)$$

where *por(x)* is the porosity of the tailings [m^3/m^3]. Therefore, by combining equations 3 and 4, the sink term for a unit volume of tailings can be written as

$$q(x,t) = \frac{\partial(\text{mass}O_2)}{\partial t} = \frac{3(1-\text{por}(x))\,D2}{R^{*3}}\left(\frac{R^* r_c^*(x)}{R^* - r_c^*(x)}\right) U_w^*(x,t) \qquad (5)$$

By combining equations 1 and 5, an expression for oxygen diffusion into tailings with the sink term represented as shrinking core particles can be written as

$$apor(x)\frac{\partial U_A^*(x,t)}{\partial t} = D1(x)\frac{\partial^2 U_A^*(x,t)}{\partial x^{*2}} - \frac{3(1-por(x))D2}{R^{*3}}\left(\frac{R^* r_c^*(x,t)}{R^* - r_c^*(x,t)}\right)U_W^*(x,t) \qquad (6)$$

Equation 6 expresses the mass balance for oxygen diffusing into the pore space of the tailings including the loss of oxygen to the particles. Because there are two variables in equation 6, $U_A^*(x,t)$ and $r_c^*(x,t)$, another equation relating these two variables is necessary in order to obtain a unique solution.

RATE OF CORE SHRINKING

An expression relating $U_A^*(x,t)$ and $r_c^*(x,t)$ can be obtained by first returning to equation 3 and observing that

$$d(\text{mass } O_2) = \varepsilon\, d(\text{mass sulfur})$$

where, ε is the mass ratio of O_2 to sulfur based on stoichiometry from

$$FeS_2 + H_2O + 7/2\, O_2 \Rightarrow FeSO_4 + H_2SO_4 \qquad (7)$$

and further noting that

$$d(\text{mass solid}) = \frac{\rho_s\, dV_{solid}}{(1-por)} = \frac{\rho_s\, d(4/3\pi\, r_c^{*3})}{(1-por)} = \frac{4\pi\, \rho_s\, r_c^{*2}\, dr_c^*}{(1-por)} \qquad (8)$$

where $\rho_s = \rho_b \times fracsulf(x)$, ρ_b is the bulk density of the tailings [kg/m^3], and $fracsulf(x)$ is the fraction of sulfur in the tailings solids [kg/kg]. Equation 3 can be rewritten as

$$\frac{dr_c^*}{dt} = \frac{D2(1-por)}{\varepsilon\, \rho_s\, r_c^{*2}}\left(\frac{R^* r_c^*(x)}{R^* - r_c^*(x)}\right)U_W^*(x,t) \qquad (9)$$

Equations 6 and 9 define a system of two equations and two unknowns; it is therefore possible to determine a unique solution for the variables $U_A^*(x,t)$ and $r_c^*(x,t)$. Equations 6 and 9 are similar to those developed by Davis and Ritchie (1986).

NUMERICAL MODEL DEVELOPMENT

Equations 6 and 9 are solved numerically using an algorithm similar to that of Davis et al. (1986). Because it was necessary to have spatially variable input parameters, a finite element scheme was chosen. Spatial variability of input parameters is easily implemented into a finite element grid by

assigning elemental properties within the domain. Because the model was developed using dimensionless equations, the dimensionless forms of equations 6 and 9 are shown below as equations 10 and 11. Details on the conversion to dimensionless form can be found in the appendix. Written in dimensionless form equation 6 becomes

$$apor(x)\frac{\partial U_A(x,t)}{\partial t} = D1(x)\frac{\partial^2 U_A(x,t)}{L^2 \partial x^2} - \frac{3(1-por(x))D2}{a^2}\left(\frac{r_c(x,t)}{1-r_c(x,t)}\right)U_W(x,t) \qquad (10)$$

and equation 9 becomes

$$\frac{dr_c}{dt} = \frac{D2(1-por)U_0}{\varepsilon \rho_s a^2}\left(\frac{1}{r_c(x) - r_c(x)^2}\right)U_W(x,t) \qquad (11)$$

where, a is the radius of an unreacted particle [m], L is the thickness of the unsaturated zone [m], and U_0 is the concentration of oxygen in the atmosphere [kg/m^3]. The variables R, $r_c(x,t)$, $U_W(x,t)$, and x are now dimensionless with values ranging from 0 to 1. Note that U_A and U_W are related through Henry's constant and are therefore not unique variables.

Numerical Formulation for Bulk Diffusion

The solution to equation 10 is achieved through the use of the Galerkin finite element technique. The matrix formulation with variable time weighting can be written as

$$\left(\theta([A]+[C])+\frac{1}{\Delta t}[B]\right)\{U_A\}_{t+\Delta t} = \left(-(1-\theta)([A]+[C])+\frac{1}{\Delta t}[B]\right)\{U_A\}_t \qquad (12)$$

where $[A]$, $[B]$, and $[C]$ are n x n coefficient matrices with n being the number of nodes. Typical matrix entries for row i and column j are

$$A_{ij} = \sum_e \int_A \frac{D1(e)}{L^2}\frac{\partial w_i}{\partial x}\frac{\partial w_j}{\partial x}\,dx,$$

$$B_{ij} = \sum_e \int_A apor(i)\, w_j w_i\,dx,$$

$$C_{ij} = \sum_e \int_A \frac{3(1-por(x))D2}{a^2} \times XHEN \times \left(\frac{r_c(x,t)}{1-r_c(x,t)}\right) w_j w_i\,dx$$

where *XHEN* is the inverse of Henry's constant for oxygen in its dimensionless form, e refers to the element, and θ is the variable time weighting term. ($0 < \theta < 1$). A θ value of 0 would give explicit time

weighting, and a value of 1 would give implicit. Typically, centered time weighting is preferred corresponding to a value of $\theta = 0.5$. Further details on the Galerkin formulation can be found in Huyakorn and Pinder (1983).

The matrices in equation 12 are set up incorporating a first-type boundary condition at the surface, and a zero concentration gradient (type II) boundary at the water table. The 1-D finite element formulation results in a left-hand side matrix with a bandwidth of 3. A Thomas algorithm is used to solve the resulting matrix .

Numerical Formulation for Rate of Core Shrinking

The solution for equation 11 is obtained through use of a Newton-Raphson technique similar to that of Davis et al. (1986). Rearranging equation 11 and integrating over one time step,

$$\int_{r_c^t}^{r_c^{t+\Delta t}} r_c(x)\,dr_c - \int_{r_c^t}^{r_c^{t+\Delta t}} r_c^2(x)\,dr_c = \frac{D2(1-por)U_0}{\varepsilon\ \rho_s\ a^2} \int_t^{t+\Delta t} \left(U_A(x,t) \times XHEN \right) dt \qquad (13)$$

The left-hand side is integrated over the integration limits given, whereas the right-hand side is integrated using the trapezoidal rule. The resulting equation is

$$\left(r_c^{t+\Delta t}(x,t)\right)^2 \left(\frac{1}{2} - \frac{r_c^{t+\Delta t}(x,t)}{3}\right) - \left(r_c^t(x,t)\right)^2 \left(\frac{1}{2} - \frac{r_c^t(x,t)}{3}\right) + con3(x)\left(U_A^t(x,t) + U_A^{t+\Delta t}(x,t)\right) = 0 \qquad (14)$$

where,

$$con3(x) = \frac{D2(1-por)U_0}{\varepsilon\ \rho_s\ a^2} \times XHEN \times \frac{dt}{2}$$

Equation 14 can now be solved using a Newton Raphson scheme. Equations 12 and 14 are solved iteratively until both $U_A(x,t)$ and $r_c(x,t)$ converge simultaneously. In order to start the iterative process for each time step, an initial estimate for $r_c(x,t)$ must be made. The estimate for each new time step is made by using a linear prediction based on the previous values of $r_c(x,t)$. The form of the prediction is

$$r_c^{t+\Delta t}(x,t) = 2\left(r_c^t(x,t)\right) - r_c^{t-\Delta t}(x,t) \qquad (15)$$

The PYROX simulation is run to a preset time or stops when all the sulfide minerals have oxidized.

REACTION PRODUCTS

The PYROX model described above was modified to facilitate coupling with the reactive transport model MINTRAN. The main modification takes into account the speciation of iron into Fe(II) and Fe(III), which is dependent on the geochemical conditions at each node in the simulation. Because the oxygen consumption by particles in the tailings differs depending on whether Fe(II) or Fe(III) is produced, the equations describing iron speciation must be incorporated in the iterative solution to U_A (x,t) and $r_c(x,t)$. The masses of H^+, SO_4^{2-}, Fe(II), and Fe(III) are calculated and then transferred to the appropriate reactive transport modules within MINTOX.

Masses of Oxidation By-products Produced

The term r_c (x,t) indicates how much of the particles are left unreacted. Because we know the original amount of sulfide minerals present, we can calculate the mass of pyrite consumed. Because r_c (x,t) is dimensionless, the fraction pyrite consumed in a unit volume of tailings can be calculated as

$$Alph(x,t) = (1 - r_c^3(x,t)) \qquad (16)$$

This value is calculated at every node and has a range from 0 to 1. The moles of sulfur consumed per unit volume of tailings can then be calculated by

$$\text{moles Sulfur} = \text{Alph}(x,t) \times \frac{\rho_s}{\text{gram formula wt. sulfur}} \qquad (17)$$

The following equations provide the stoichiometry necessary to calculate the number of moles H^+, SO_4, Fe(II), and Fe(III) produced per mole of sulfur oxidized in pyrite.

$$FeS_2 + H_2O + 7/2\ O_2 \Rightarrow Fe^{2+} + 2SO_4^{2-} + 2H^+ \qquad (18)$$

$$FeS_2 + 1/2H_2O + 15/4\ O_2 \Rightarrow Fe^{3+} + 2SO_4^{2-} + H^+ \qquad (19)$$

Equation 18 describes the reaction when iron produced is in the form Fe(II), whereas equation 19 describes the reaction in the case where Fe(II) has been oxidized to Fe(III).

If the Fe(II) produced in equation 18 is oxidized by oxygen, it oxidizes according to the following reaction:

$$Fe^{2+} + 1/4O_2 + H^+ \Rightarrow Fe^{3+} + 1/2H_2O \qquad (20)$$

This reaction consumes oxygen and therefore would act as an additional sink for oxygen in the pore space of the tailings. To account for both Fe(II) and Fe(III) being produced due to pyrite oxidation, the sink term in the subroutine PYROX must be modified.

From the stoichiometry of equation 18 or equation 19 it is possible to determine the total amount of iron produced (Fe^{total}) once the mass of sulfur produced due to the oxidation of the sulfide mineral is known. The oxygen concentration in the pore space that is calculated in the subroutine PYROX is dependent on whether Fe(II) or Fe(III) is produced. Because the pH, the speciation of the iron, and the consumption of oxygen are interdependent, an iterative approach must be taken. The following relationship can be derived based on the equilibrium assumption:

$$\log\left(\frac{a_{Fe^{3+}}}{a_{Fe^{2+}}}\right) = \mathrm{Log}(K_{eq}) + \frac{1}{4}\mathrm{Log}(P_{O_2}) - \mathrm{pH} \qquad (21)$$

where a_{Fe}^{3+} and a_{Fe}^{2+} are the activities of Fe(III) and Fe(II) and K_{eq} is the equilibrium constant for iron. The total amount of iron produced will be equal to the sum of Fe(II) and Fe(III) as

$$Fe^{total} = Fe(II) + Fe(III) \qquad (22)$$

Combining equations 21 and 22, assuming concentrations and activities are equivalent, and replacing the partial pressure of oxygen with the concentration of oxygen in the pore water ($U_W(x,t)$) leads to the following equation:

$$\left(\frac{[Fe(II)]}{[Fe^{total}]}\right) = 1/[(K_{eq}) \times (U_W)^{1/4} \times 10^{-pH} + 1] \qquad (23)$$

These calculations are made using a constant temperature of 25°C. If temperature variations are significant, adjustments could be made accordingly.

Equations 10 and 11 along with equations 22 and 23 form a system of four equations and four unknowns. The variables that are unknown in these equations are $U_A(x,t)$, $r_c(x,t)$, Fe(II), and Fe^{total}. All four must converge simultaneously within each time step.

The algorithm used in the model PYROX was modified to accommodate the speciation of Fe(II) and Fe(III) as follows:

i) Solve for $U_W(x,t)$ in equation 10 starting with an initial guess of $r_c(x,t)$.

ii) Solve for $r_c(x,t)$ in equation 11 using $U_W(x,t)$ from part *i*.

iii) Calculate ratio of Fe(II) to Fe^{total} using equation 23 with pH from the equilibrium chemistry module (MINTEQA2) and the oxygen concentration calculated in *i*.

iv) Calculate the new ratio for mass of oxygen consumed to sulfur produced ($\varepsilon(x,t)$) based on whether Fe(II) or Fe(III) is produced during the time step for all nodes. This value is used to calculate the sink term for oxygen.

v) Repeat step *i* using the new values calculated in steps *ii*, *iii*, and *iv*.

vi) Repeat steps *i* to *v* until $U_W(x,t)$, $r_c(x,t)$, Fe(II), and Fe^{total} have all converged. Convergence criteria are based on changes in $r_c(x,t)$ between iterations.

vii) Predict next value for $r_c(x,t)$ using equation 15.

viii) Move to next time step.

LINKING REACTIVE TRANSPORT TO PYRITE OXIDATION MODEL (MINTOX)

The reactive transport model MINTRAN is capable of functioning as either a 1-D or 2-D model, whereas the oxygen diffusion model PYROX is strictly one-dimensional. The two models are coupled together in such a way that MINTOX is capable of running either a 1-D simulation of a column experiment or a 2-D field-scale simulation where the oxygen diffusion is assumed to occur only in the vertical direction.

Figure 3 shows the nodal and elemental numbering scheme for the reactive transport modules and for the oxygen-diffusion module. The domain over which the reactive transport part of the code operates includes both the saturated and unsaturated zone, whereas the oxygen diffusion code operates only in the unsaturated zone with the water table forming its lower boundary. The aqueous products of pyrite oxidation are allowed to react with all other aqueous and solid components in both the saturated and unsaturated zones.

As the program MINTOX marches through time, the degree of pyrite oxidation occurring within the current time step is calculated. The oxidation of pyrite produces H^+, SO_4, Fe(II), and Fe(III). The concentration of these reaction products is calculated at each node in the unsaturated zone and then added to the corresponding spatial node in the reactive transport portion of the code. The entire set of aqueous components are individually transported, and the solid and aqueous chemistry is equilibrated at each node. The program moves on to the next time step, and oxidation of pyrite continues. If the pyrite at any location in the unsaturated zone is completely depleted, the program calculates a zero concentration increase at that point in space for all the reaction products.

MODEL EVALUATION

The reactive transport model MINTRAN has been evaluated by Walter et al. (1994a) for nonlinear ion exchange using data from Valocchi et al. (1981) and a 1-D mine-tailings simulation. For the latter, Walter et al. (1994a) compared results from MINTRAN to those derived using PHREEQM (Appelo and Willemsen, 1987).

In order to evaluate the MINTOX model, a 1-D column simulation was performed using solid and aqueous chemistry from the Nordic Main tailings impoundment near Elliot Lake Ontario. The model was set up to simulate the effects of 12 years of pyrite oxidation based on physical and chemical data acquired at the site. The data were taken from Smyth (1981), and Dubrovsky (1986). The field location T3 was chosen for modelling because of the large unsaturated zone and abundance of data available from that location. However, not all the necessary data required for proper model evaluation were available.

Geochemical Setting and Boundary Conditions for 1-D Simulation

The Nordic Main tailings at Elliot Lake were deposited from 1957 to 1968. Prior to deposition the tailings were treated with lime and limestone, resulting in a slurry with a pH of 8. In 1972, lime and crushed limestone were added to the surface of the tailings along with fertilizers, and a program of vegetation was initiated. Smyth (1981) collected data from the site in 1980 and 1981 allowing for approximately 12 years of oxidation to occur prior to data collection.

A 6-metre-long by 0.1-metre-wide column simulation was run using solid and aqueous data collected at site T3. Time-invariable moisture-content and porosity data were input into the PYROX subroutine to calculate the spatially variable bulk diffusion coefficients for oxygen within the column.

For the PYROX subroutine the surface was considered a first-type boundary with the oxygen concentration equal to the atmospheric concentration of oxygen. The bottom boundary was considered the top of the water table, which constitutes a zero concentration gradient (second-type) boundary condition for the diffusion of oxygen. Because the tailings are snow-covered for 5 months of the year, the diffusion of oxygen into the tailings was assumed to be seasonal and occurring for only 7 months of the year.

For the reactive transport portion of the model, the upper boundary was a third-type boundary with a constant water flux of 0.31 m/yr, which is consistent with estimated recharge (Dubrovsky, 1986). The chemistry of the influx water from the surface was originally considered similar to rainwater in the region; however, the concentrations were modified based on discrepancies between modelled output and field data. This was required because unknown quantities of lime, fertilizer, and sewage sludge were added to the surface of the tailings during revegetation attempts (Smyth, 1981). Influx chemistry is listed in Table 1. All other boundaries were assumed to be zero-dispersive-flux Neuman-type (second type).

The velocity of water flow was considered constant at 0.62 m/yr based on the influx rate and a constant porosity of 0.5, and it is consistent with that found by Dubrovsky (1986). The Peclet and Courant criteria were satisfied for all simulations, and a longitudinal dispersivity of 0.1 metres was used throughout.

The solid-phase components and the geochemical reactions incorporated in the simulations were drawn from the conceptual model of the geochemical evolution of the Nordic uranium tailings developed by Smyth (1981) and Dubrovsky (1986). This conceptual model included a series of pH-buffering, mineral-dissolution reactions, including calcite dissolution, siderite dissolution, and the dissolution of ferric and aluminum hydroxides. This conceptual model was developed using pore-water chemistry data and the geochemical speciation model WATEQ2 (Ball et al., 1980). Although the presence of these

mineral buffers within the tailings was not confirmed by mineralogical study, carbonate contents were determined through chemical analysis and ferric hydroxide phases visible in the samples of the tailings. Initial estimates of the mineralogy and the solid phase concentrations were based on previous modelling done by Walter et al. (1994a) and Dubrovsky (1986). The pH-buffering minerals included in the simulation are calcite, siderite, $Al(OH)_3$, and $Fe(OH)_3$. These phases are consistent with those inferred at the Nordic site and at several other mine-tailings impoundments (Smyth, 1981; Dubrovsky et al., 1984; Blowes and Ptacek, 1994). In addition to the buffering reactions previously modelled by Dubrovsky (1986) and Walter et al. (1994b), jarosite ($KFe_3(SO_4)_2(OH)_6$) was included.

Amorphous silica is included in the 1-D simulations because it is the form of silica most likely to attain equilibrium. Since it is unlikely that complete dissolution of amorphous silica in the tailings would occur, an arbitrarily large input concentration was chosen to ensure that it did not completely dissolve. The dissolution and precipitation of other silicate minerals will be kinetically limited and therefore are not included.

Aluminosilicate minerals were not included in the 1-D simulations even though dissolution of aluminosilicates may be an important acid-neutralization mechanism in tailings. The aluminosilicate dissolution reactions are frequently slower than the rate of pore-water movement within the tailings (Blowes and Ptacek, 1994) and thus would not be modelled correctly using an equilibrium approach. In addition, the thermodynamic data for these minerals included in the MINTEQA2 database were obtained from high-temperature, free-energy studies. Use of these data to predict mineral stability at low temperatures should be viewed with caution. The exclusion of aluminosilicate minerals from the MINTOX simulations will lead to errors in predictions of aqueous concentrations of dissolved species derived from these minerals; e.g., Al, Si, K, Na. As a result of this assumption the model MINTOX is not well suited to modelling the geochemical evolution of tailings that are devoid of carbonate and hydroxide minerals.

The rate at which pH-buffering fronts move is directly related to the solid phase concentration of the buffering minerals in the tailings. The concentrations of the buffering mineral phases in the Elliot

Lake tailings are not known and therefore had to be estimated. The concentrations of these minerals were adjusted in each successive run of MINTOX until a reasonable fit to the field data was achieved. The various input parameters used in the simulations are listed in Tables 2 to 4 and the pH-buffering reactions and species included in the simulation are listed in Tables 5 and 6.

Oxygen Transport 1-D Simulation Results from PYROX

The first step in modelling the Elliot Lake data was to run the pyrite oxidation model, PYROX, to obtain a reasonable match between the model output and the field data. Figure 4 shows the normalized oxygen concentration versus depth profile and normalized sulfur content for the modelled output and field data. The oxidation front in the tailings has progressed to a maximum depth of about 0.9 metres (Figure 5). Slight modifications were made to the moisture-content data in the upper 0.5 metres of the tailings due to unusually wet conditions at site T3 during collection of the moisture-content data (D.J.A. Smyth, personal communication). The oxygen concentration at the surface is equal to the atmospheric concentration of oxygen and decreases gradually to a depth of 0.7 metres. Below this depth, the oxygen concentration rapidly decreases, where it reaches the detection limit at a depth of approximately 0.9 metres. The zone between 0.7 and 0.9 metres is where oxygen is most rapidly consumed by pyrite oxidation. The fraction of pyrite remaining shows the reverse trend. Pyrite is depleted near the surface and the pyrite content increases to background levels between 0.7 and 0.9 metres.

MINTOX 1-D Simulation Results

The general trends observed in the modelled results correspond well with those of the field data (Figures 6 through 8). The pH profile shown has several zones where the pH is buffered by different mineral phases (Figure 6). In the near surface zone, the pH is buffered by jarosite precipitation and dissolution at a pH of about 2.0. Below the jarosite-buffered zone ferrihydrite buffers the pH to approximately 2.7, followed by gibbsite at a pH of approximately 3.7, siderite at a pH of around 4.5, and finally calcite in the deepest section at a pH of approximately 5.9. Iron concentrations show two distinct peaks (Figure 7). The upper peak in the ferrihydrite buffered zone consists mostly of Fe(III), whereas the lower peak in the

zone where gibbsite is the buffering mineral consists mostly of Fe(II). Below a depth of 3 metres the modelled and field results of Fe^{total} concentrations differ substantially (Figure 7). Within this zone the pH of the field data is relatively constant at about 6. Geochemical calculations suggest that the pH in this zone is buffered by calcite. However, equilibrium calculations using MINTEQA2 show that under these geochemical conditions, the presence of calcite causes concentrations of Fe(II) to be lower than those observed in the field due to precipitation of siderite. Although a number of attempts were made to reconcile these differences, it was not possible to obtain high Fe(II) concentrations while maintaining equilibrium with respect to calcite. Possible explanations for this discrepancy are that calcite is not the buffering mineral in this zone, or that calcite or siderite are present as a solid solution, containing impurities, rather than the pure phase. The physio-chemical relations between solid solutions and aqueous solutions are not included in MINTOX. Another possible explanation is that kinetic limitations may be preventing siderite from precipitating. If the system were not in equilibrium with respect to siderite, then Fe(II) concentrations would be higher than those calculated using an equilibrium approach. Reaction kinetics, except those involving pyrite, are not presently included in MINTOX but should be incorporated in future work.

Geochemical Setting and Boundary Conditions for 2-D Simulation

Two-dimensional simulations were run to show the ability of the MINTOX model to simulate physical and chemical changes imposed on tailings impoundments and to show that these changes may have profound effects on the resulting acid and contaminant generation caused by the oxidation of sulfide minerals. The hypothetical 2-D simulations are loosely based on the solid and aqueous chemistry from the Nordic tailings impoundment, Elliot Lake. The grid and velocity vectors were generated using the Waterloo Hydrogeologic Software program FLONET. The grid dimensions are 25 metres horizontally by 7 metres vertically. The upper 1.5 metres of the domain are unsaturated and the remainder fully saturated with a constant porosity of 0.5. For simplicity the velocities in the unsaturated zone were assumed to be vertical (Figure 9). Longitudinal and transverse dispersivity values of 2.0 and 0.05 metres respectively were used throughout the domain.

For the PYROX subroutine the surface was considered to be a first-type boundary with the oxygen concentration equal to the atmospheric concentration of oxygen. The bottom boundary is the top of the water table that constitutes a zero concentration gradient (second-type) boundary condition for the diffusion of oxygen. The diffusion of oxygen into the tailings was considered seasonal, occurring only half the year, and assumed to occur in only one dimension.

For the 2-D simulations the pH buffering reactions chosen were similar to the 1-D simulations (Table 5), with the exception that precipitation and dissolution of jarosite and amorphous silica, which were not included. The various input parameters used in the simulations are listed in Tables 7 through 10. Species included in the 2-D simulations are the same as those in the 1-D simulation (Table 6) with the exclusion of the magnesium and silicate species. For the simulations, it was assumed that sulfide minerals were contained only in a 10-metre-wide segment of the unsaturated zone.

Initial Scenario

Initially the simulation was run for an oxidation period of 10 years. Because chloride (Cl) is assumed to be a non-reactive component in the simulation, it will define the extent of the plume emanating from the tailings (Figures 10 and 11). The other aqueous component plots show varying amounts of retardation. There is a strong correlation between aqueous phases and solid phases. The low-pH plume has progressed to the point where background calcite has dissolved. In the upper section of the tailings, Fe(III) concentrations are controlled by ferrihydrite precipitation and dissolution. Beneath the ferrihydrite buffered zone, aluminum concentrations are controlled by precipitation and dissolution of gibbsite, followed by a zone where Fe(II) concentrations are controlled by precipitation and dissolution of siderite. Beyond the siderite buffered zone, calcite is the principal pH-buffering mineral, and the pH is constant at approximately 6. The concentrations of Fe(III) are high in the unsaturated zone where oxygen is present in the pore space, and decrease rapidly below the water table. The concentrations of Fe(II) show the opposite effect; low concentrations are seen in the unsaturated zone and higher concentrations below the water table.

Moisture Retaining Cover

To show the sensitivity of the oxidation process to the moisture content of the tailings, a simulated cover was placed on the tailings at time zero. The cover is hypothetical in the fact that only the moisture content of the cover was altered. In reality a cover engineered to retain the same moisture content as the modelled cover would have a different hydraulic conductivity, porosity, and bulk density. Changes in these parameters would change the flow field within the tailings; thus, the effects of the increased moisture content alone would be difficult to discern. Moisture content within the cover was increased to 0.44, with the total porosity 0.50. All other properties in the cover, including sulfur content, remained the same as the tailings. The modelled thickness of the cover was 18 cm or 3 elements.

The results after 10 years of oxidation show that the Cl plume has been unaffected by the addition of the cover because the flow field has not been altered (Figure 12). The development of the other aqueous and solid-phase plumes is substantially less. Oxidation of pyrite still occurs, but the rate of contaminant loading and acid generation is much lower. It may be possible to slow the oxidation rate enough so that the rate of contaminant release into the natural environment will not cause serious environmental damage; however, because pyrite oxidation rates within tailings are highest shortly after deposition, once a large mass of pyrite has oxidized, the addition of a cover may have limited success in reducing the acid drainage problem. The MINTOX model also could be used as a tool in determining the effectiveness of adding a cover to tailings that have already undergone partial oxidation.

Limestone Addition During Deposition

A 10-year simulation was run to show the effects of limestone addition to the tailings during deposition. The amount of limestone added to the tailings for this simulation was 1.6 weight percent, giving a total limestone content of 2.0 weight percent distributed evenly throughout the tailings. The evolution of the Cl plume is unaffected by the addition of limestone (Figure 13). The neutralization of acidity results in higher pH values, which in turn enhances the precipitation of mineral phases and subsequent removal of aqueous component masses from solution. The aqueous component

concentrations show that after 10 years the majority of the plume mass remains almost entirely within the unsaturated zone (Figure 13).

CONCLUSIONS

Oxygen diffusion and pyrite oxidation in a nonhomogeneous medium was simulated using the numerical model PYROX, a shrinking-core oxidation model using a finite element numerical method. PYROX is capable of modelling the oxidation of pyrite in tailings environments where moisture content, porosity, bulk density, and pyrite content are spatially variable. Comparisons of PYROX simulations with field measured gas-phase oxygen concentrations and solid-phase sulfur contents after 12 years of sulfide oxidation show good agreement. These results suggest that PYROX may be suitable for predicting the long-term release of Fe, SO_4^{2-}, and H^+ to the pore waters of sulfide-rich tailings impoundments through sulfide oxidation reactions.

PYROX has been coupled with the reactive transport model MINTRAN using an iterative technique whereby the speciation of iron into Fe(II) and Fe(III) and the calculation of the oxygen concentration in the pore space are linked. The resulting model, MINTOX, is capable of modelling the kinetically limited oxidation of pyrite and the subsequent reactive transport of the oxidation products within the unsaturated and saturated zones of tailings impoundments. The chemical reactions described by the MINTRAN program are subject to the local equilibrium assumption, and it is assumed that acid neutralization and attenuation of dissolved metals within the tailings can be attributed to equilibrium reactions.

The results of 1-D simulations of conditions similar to those observed at the Nordic tailings impoundment near Elliot Lake, Ontario, correspond closely to field data. Calculations of aqueous component concentrations made using MINTOX closely matched general trends observed in the water chemistry after 12 years of oxidation had occurred. Some discrepancies observed may be a result of solid solutions that are unaccounted for, or reaction kinetics that are not dealt with using the equilibrium

approach. The results for the 2-D simulations show that physical and chemical changes imposed on tailings impoundments through proposed remediation programs may have profound effects on the resulting acid and contaminant generation caused by the oxidation of sulfide minerals.

REFERENCES

Appelo, C.A.J., and A. Willemsen, Geochemical calculations and observations on saltwater intrusion, A combined geochemical/mixing cell model, *J. Hydrol., 94*, 313-330, 1987.

Ball, J.W., D.K. Nordstrom, and E.A. Jenne, Additional and revised thermochemical data and computer code for WATEQ2-A computerized chemical model for trace and major element speciation and mineral equilibria of natural waters, 109 pp., U.S. Geological Survey - Water-Resources Investigations 78-116, 1980.

Blowes, D.W., and C.J. Ptacek, Acid-neutralization mechanisms in inactive mine tailings, in *Short Course Handbook on Environmental Geochemistry of SulfideMine-Wastes*, edited by J.L. Jambor and D.W. Blowes, 22, pp. 271-292, Mineralogical Association of Canada, Nepean, Ont., Canada, 1994.

Borden, R.C., and P.B. Bedient, Transport of dissolved hydrocarbons influenced by oxygen-limited biodegradation 1. Field application, *Water Resour. Res., 22*(13), 1973-1982, 1986.

Carnahan, C.L., Coupling of precipitation-dissolution reactions to mass diffusion via porosity changes, in *Chemical Modeling of Aqueous Systems II*, edited by D.C. Melchior and R.L. Bassett, *416*, pp. 234-242, American Chemical Society, Washington, D.C., 1990.

Cathles, L.M., and J.A. Apps, A model of the dump leaching process that incorporates oxygen balance, heat balance, and air convection, *Metal Trans., 6B*, 617-624, 1975.

Cathles, L.M., Predictive capabilities of a finite difference model of copper leaching in low grade industrial sulfide waste dumps. *Mathematical Geology, 11*(2), 175-191, 1979.

Davis, G.B., Mathematical modelling of rate-limiting mechanisms of pyrite oxidation in overburden dumps, Ph.D. thesis, 159 pp., Univ. of Wollongong, 1983.

Davis, G.B., and A.I.M. Ritchie, A model of oxidation in pyritic mine wastes: part 1: equations and approximate solution, *Applied Mathematical Modelling, 10*, 314-322, 1986.

Davis, G.B., G. Doherty, and A.I.M. Ritchie, A model of oxidation in pyritic mine wastes: part 2: comparison of numerical and approximate solutions, *Applied Mathematical Modelling, 10*, 323-329, 1986.

Dubrovsky, N.M., Geochemical evolution of inactive pyritic tailings in the Elliot Lake Uranium District, Ph.D. thesis, 373 pp., Univ. of Waterloo, Waterloo, Ont., Canada, 1986.

Dubrovsky, N.M., J.A. Cherry, E.J. Reardon, and A.J. Vivyurka, Geochemical evolution of inactive pyritic tailings in the Elliot Lake Uranium District., *Canadian Geotechnical Journal, 22*, 110-128, 1984.

Elberling, B., R.V. Nicholson, and J.M. Scharer, A combined kinetic and diffusion model for pyrite oxidation in tailings: a change in controls with time, *Journal of Hydrology, 157*, 47-60, 1994.

Frind, E.O., W.H.M. Duynisveld, O. Strebel, and J. Boettcher, Modeling of multicomponent transport with microbial transformation in groundwater: the Fuhrberg case, *Water Resour. Res.*, 26(8), 1707-1719, 1990.

Huyakorn, P.S., and G.F. Pinder, *Computational Methods in Subsurface Flow*, Academic, Orlando, Fla., 1983.

Jaynes, D.B., A.S. Rogowski, and H.B. Pointe, Acid mine drainage from reclaimed coal strip mines 1. Model description, *Water Resour. Res.*, *20*(2), 233-242, 1984a.

Jaynes, D.B., H.B. Pointe, and A.S. Rogowski, Acid mine drainage from reclaimed coal strip mines 2. Simulation results of model, *Water Resour. Res.*, *20*(2), 243-250, 1984b.

Jennings, A.A., D.J. Kirkner, and T.L. Theis, Multicomponent equilibrium chemistry in groundwater quality models, *Water Resour. Res.*, *18*(4), 1089-1096, 1982.

Kinzelbach, W., W. Schäfer, and J. Herzer, Numerical modeling of natural and enhanced denitrification processes in aquifers, *Water Resour. Res.*, *27*(6), 1123-1135, 1991.

Levenspiel, O., *Chemical Reaction Engineering*, J. Wiley and Sons, New York, 1972.

Lichtner, P.C., Continuum model for simultaneous chemical reactions and mass transport in hydrothermal systems, *Geochim. Cosmochim. Acta*, *49*, 779-800, 1985.

MacQuarrie, K.T.B., E.A. Sudicky, and E.O. Frind, Simulation of biodegradable organic contaminants in groundwater 1. Numerical formulation in principal directions, *Water Resour. Res.*, *26*(2), 207-222, 1990.

MacQuarrie, K.T.B., and E.A. Sudicky, Simulation of biodegradable organic contaminants in groundwater 2. Plume behavior in uniform and random flow fields, *Water Resour. Res.*, *26*(2), 223-239, 1990.

Miller, C.W., and L.V. Benson, Simulation of solute transport in a chemically reactive heterogeneous system: model development and application, *Water Resour. Res.*, *19*(2), 381-391, 1983.

Molz, F. J., M.A. Widdowson, and L. D. Benefield, Simulation of microbial growth dynamics coupled to nutrient and oxygen transport in porous media, *Water Resour. Res.*, *22*(8), 1207-1216, 1986.

Pantelis, G., and A.I.M. Ritchie, Macroscopic transport mechanisms as a rate limiting factor in dump leaching of pyritic ores. *Applied Mathematical Modelling*, *15*, 136-143, 1991.

Reardon, E.J., and P.M. Moddle, Gas diffusion coefficient measurements on uranium mill tailings: implications to cover layer design, *Uranium*, *2*, 111-131, 1985.

Rubin, J., and R.V. James, Dispersion-affected transport of reacting solutes in saturated porous media: Galerkin method applied to equilibrium-controlled exchange in unidirectional steady water flow, *Water Resour. Res.*, *9*(5), 1332-1356, 1973.

Smyth, D.J.A., Hydrogeological and geochemical studies above the water table in an inactive uranium tailings impoundment near Elliot Lake, Ontario, M.Sc. project, 72 pp., Univ. of Waterloo, Waterloo, Ont., Canada, 1981.

Steefel, C.I., and A.C. Lasaga, Evolution of dissolution patterns, permeability change due to coupled flow and reaction, in *Chemical Modeling of Aqueous Systems II*, edited by D.C. Melchior and R.L. Bassett, *416*, pp. 213-225, American Chemical Society, Washington, D.C., 1990.

Valocchi, A.J., R.L. Street, and P.V. Roberts, Transport of ion-exchanging solutes in groundwater: chromatographic theory and field simulation, *Water Resour. Res.*, *17*(5), 1517-1527, 1981.

Walter, A.L., E.O. Frind, D.W. Blowes, C.J. Ptacek, and J.W. Molson, Modelling of multicomponent reactive transport in groundwater 1. Model development and evaluation, *Water Resour. Res.*, *30* (11), 3137-3148, 1994a.

Walter, A.L., E.O. Frind, D.W. Blowes, C.J. Ptacek, and J.W. Molson, Modelling of multicomponent reactive transport in groundwater 2. Metal mobility in aquifers impacted by acidic mine tailings discharge, *Water Resour. Res.*, *30*(11), 3149-3158, 1994b.

Yeh, G.T., and V.S. Tripathi, A critical evaluation of recent developments in hydrogeochemical transport models of reactive multichemical components, *Water Resour. Res.*, *25*(1), 93-108, 1989.

Zysset, A., F. Stauffer, and T. Dracos, Modelling of reactive groundwater transport systems. Part I. General kinetic and equilibrium formulation, *Water Resour. Res.*, in press, 1994a.

Zysset, A., F. Stauffer, and T. Dracos, Modelling of reactive groundwater transport systems. Part II. Kinetic formulation of a system governed by biodegradation, *Water Resour. Res.*, in press, 1994b.

LIST OF FIGURES

LIST OF TABLES

Figure 1. Two-stage oxidation process for pyrite oxidation in a tailings impoundment. Oxygen diffuses into bulk pore space, partitions into water film, and then diffuses into pyrite grains through the oxidized coating formed around the unoxidized core.

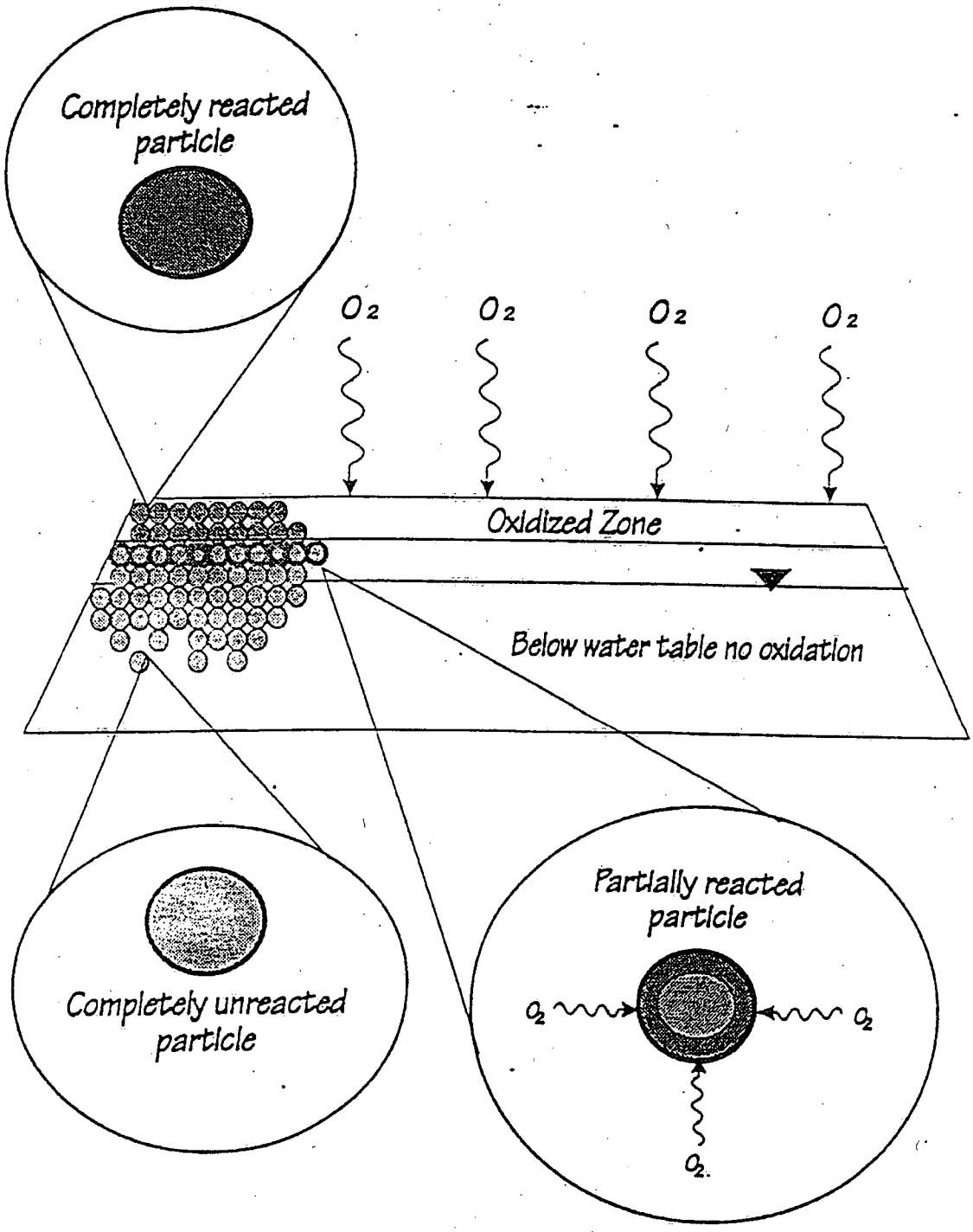

Figure 2. Partially oxidized pyrite grain. Oxygen concentration gradient between surface of particle and unreacted core causes oxygen to diffuse into particle.

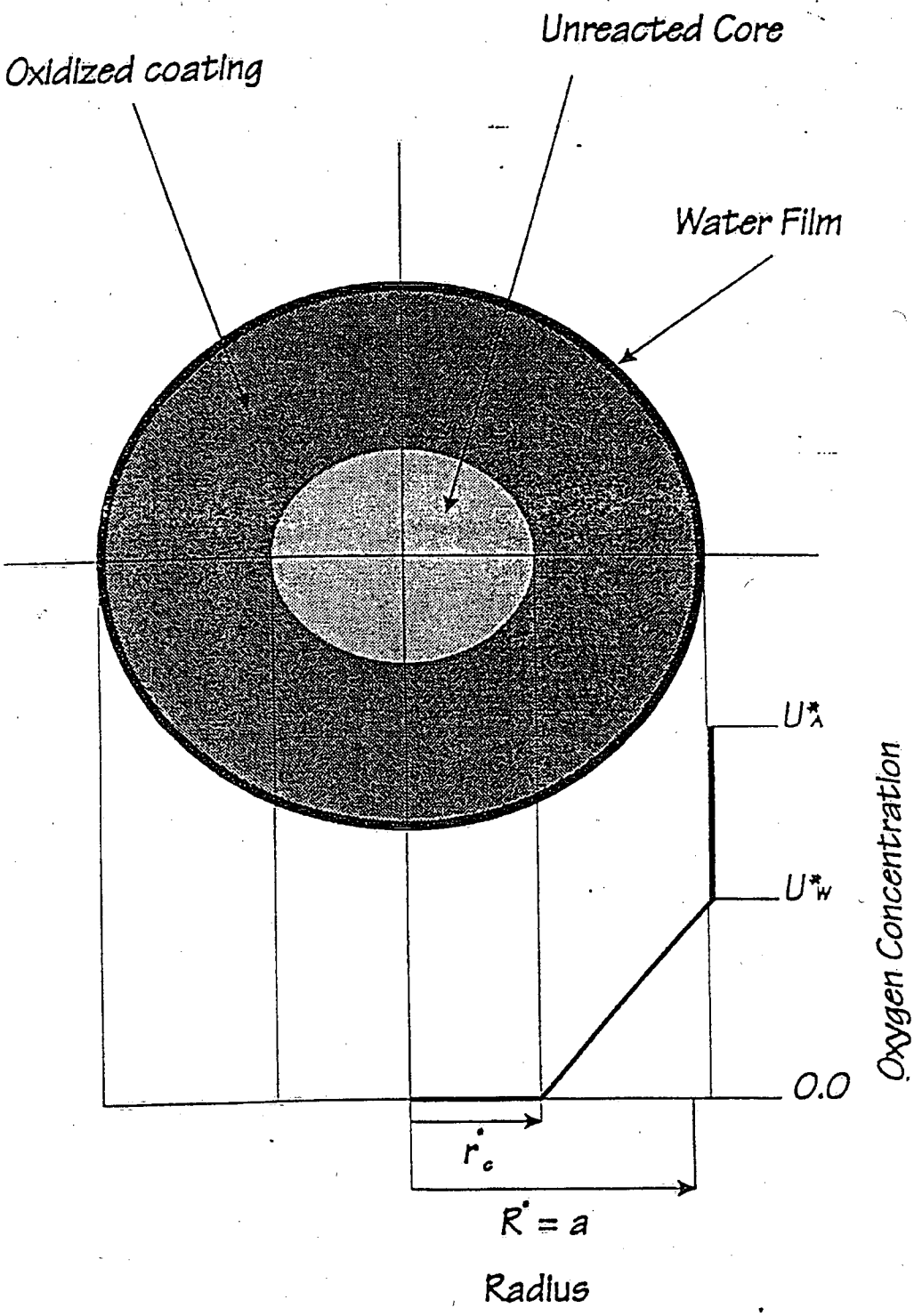

Figure 3. Nodal and elemental numbering for PYROX subroutine and MINTRAN.

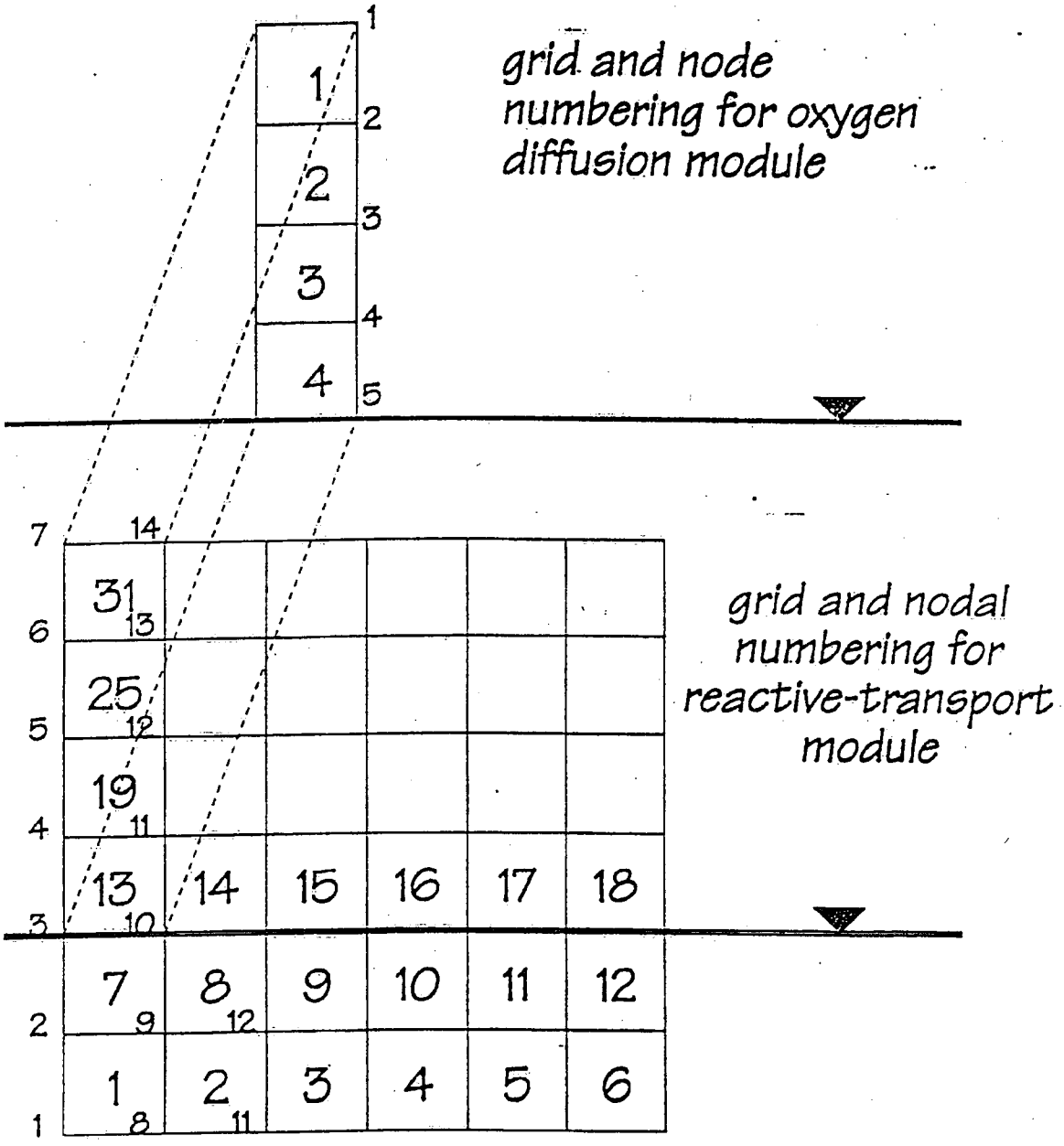

Figure 4. Field and modelled oxygen concentrations from the Nordic mine-tailings impoundment at Elliot Lake, Ontario, piezometer nest location T3. Field data from Smyth, (1981).

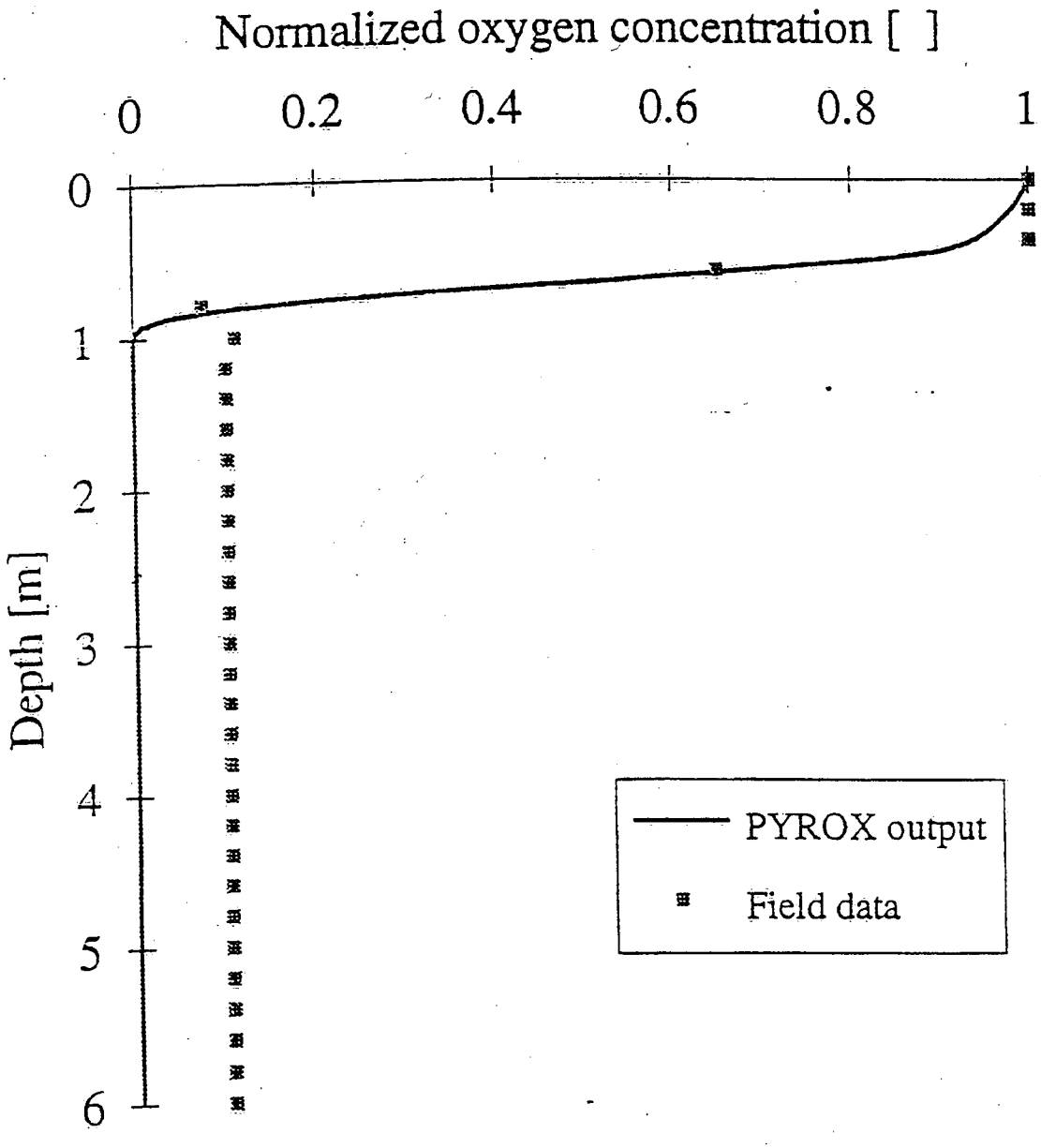

Figure 5. Field and modelled pyrite concentrations from the Nordic mine-tailings impoundment at Elliot Lake, Ontario, piezometer nest location T3. Field data from Smyth, (1981).

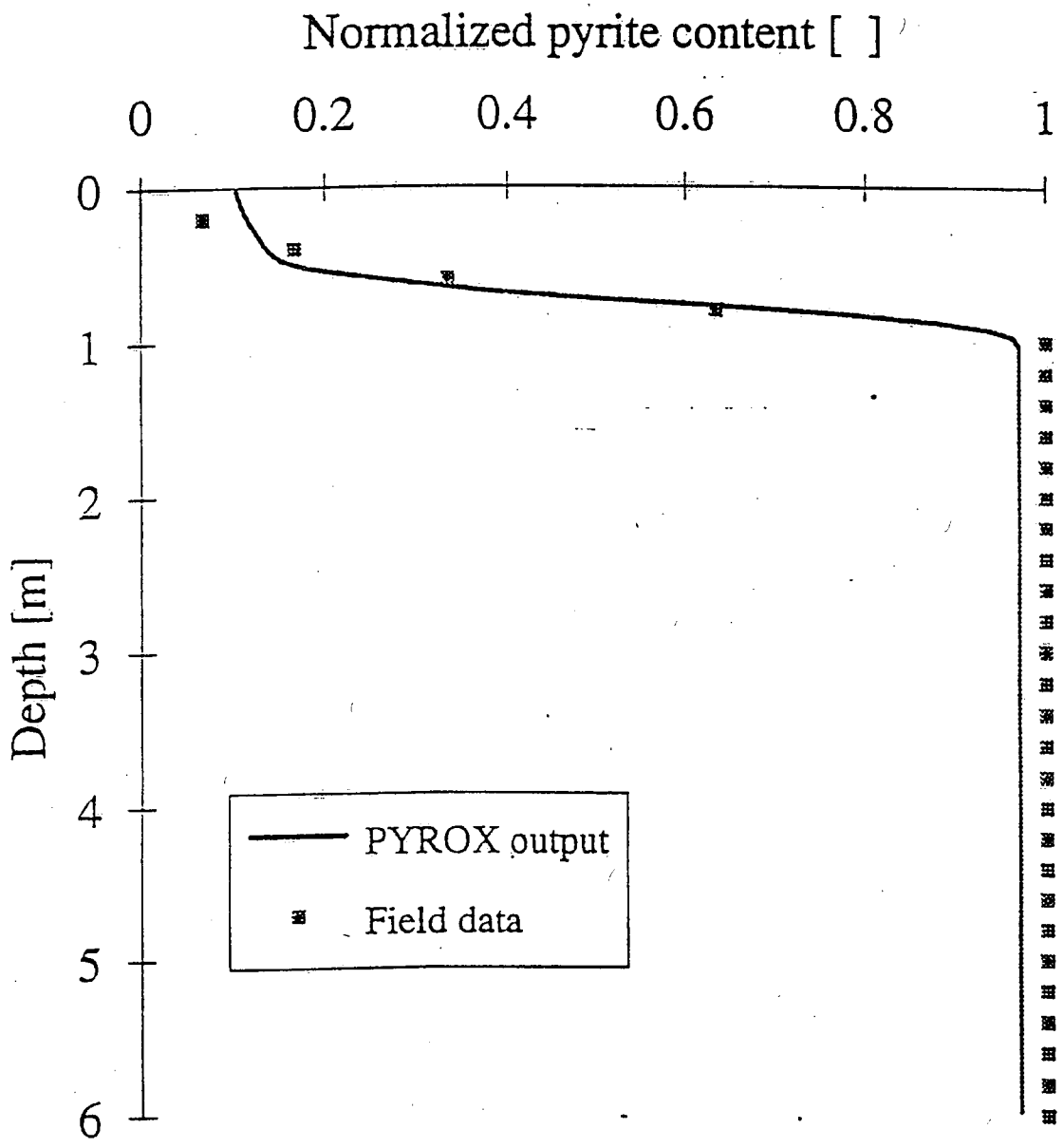

Figure 6. 1-D simulation results. Solid lines are modelled results, squares are field data from the Nordic mine-tailings impoundment at Elliot Lake, Ontario, piezometer nest location T3. Field data collected in May, 1981. Field data from Smyth (1981).

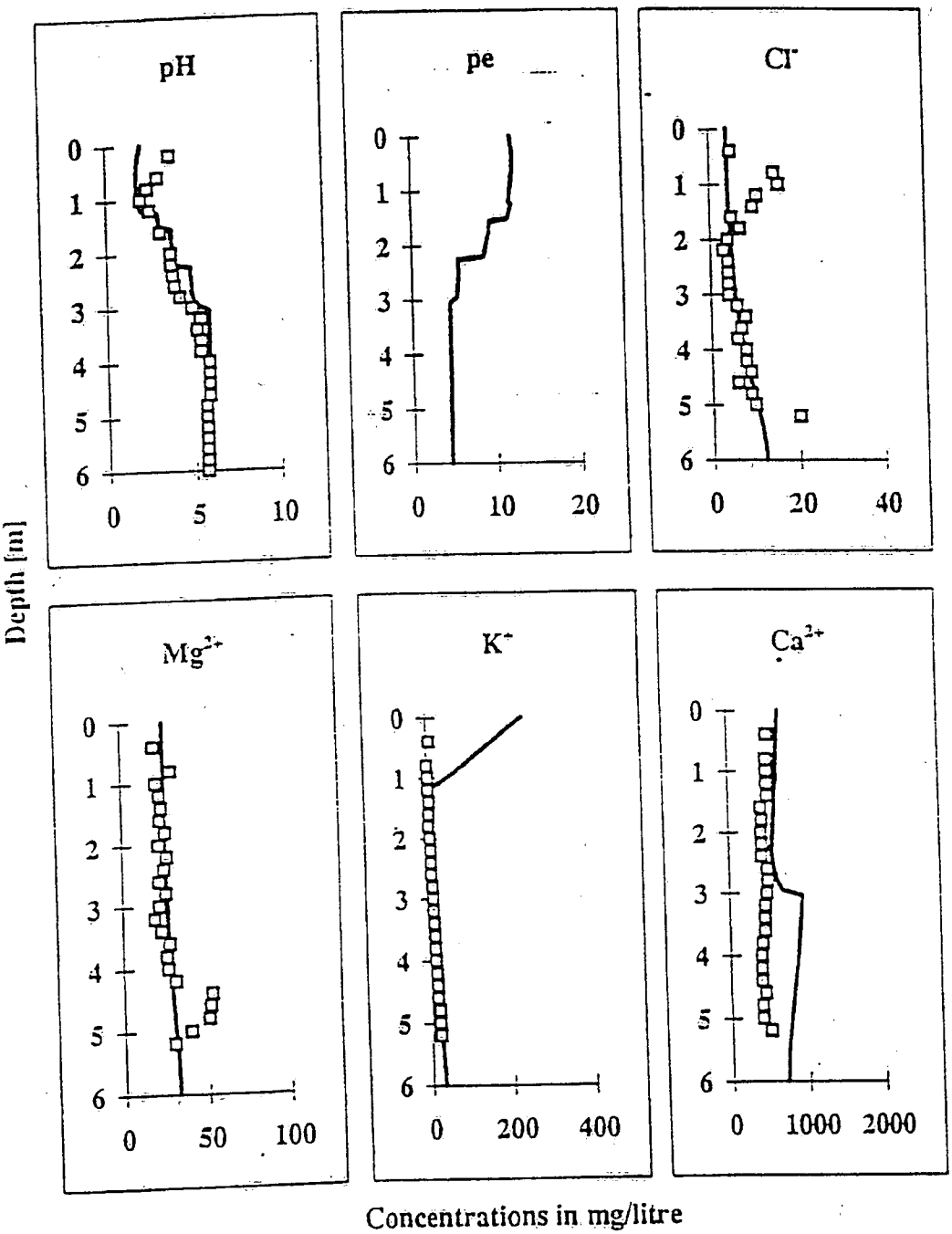

Figure 7. 1-D simulation results (cont.). Solid lines are modelled results, squares are field data from the Nordic mine-tailings impoundment at Elliot Lake, Ontario, piezometer nest location T3. Field data collected in May, 1981. Field data from Smyth (1981).

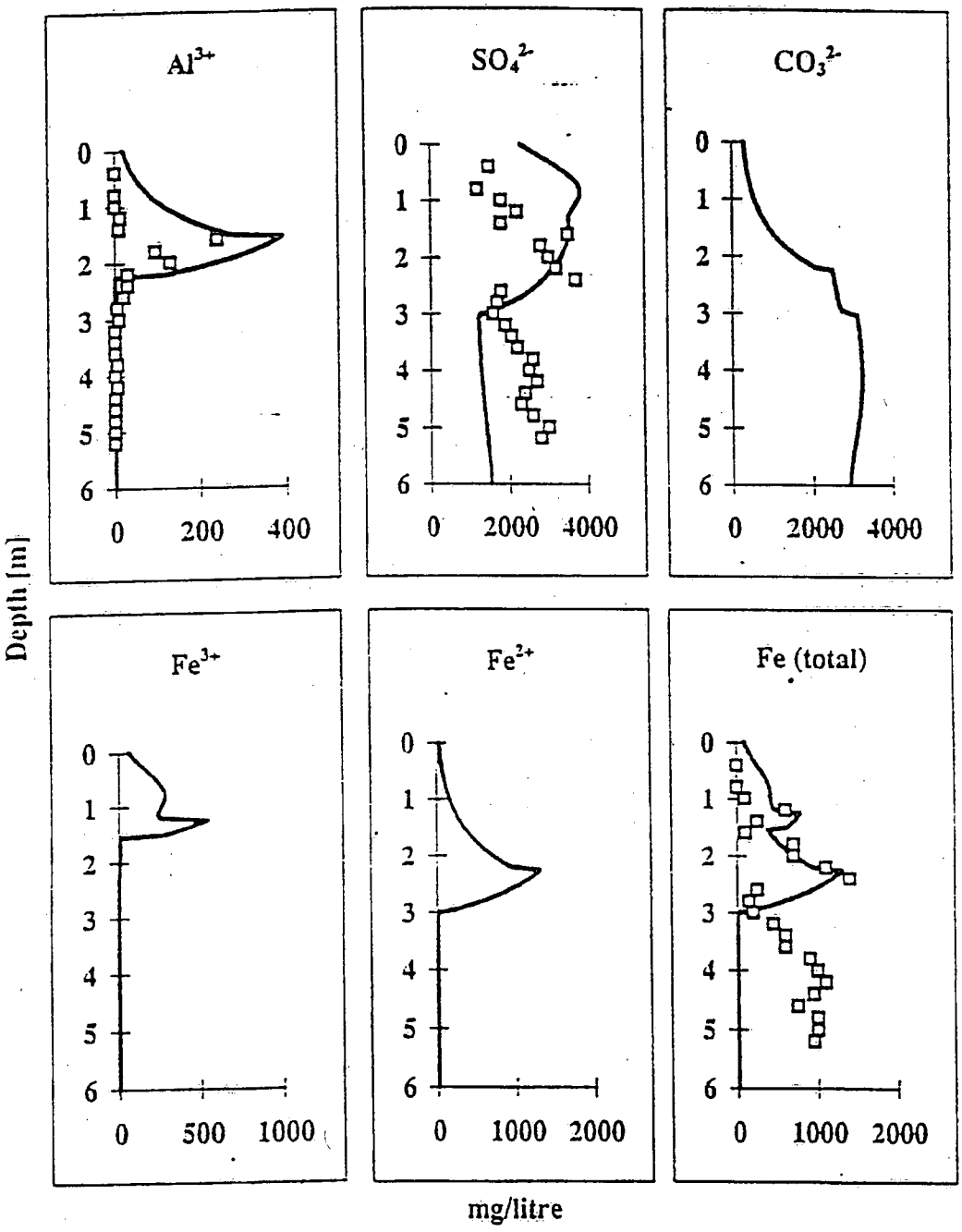

Figure 8. 1-D simulation results (cont.). Solid lines are modelled results.

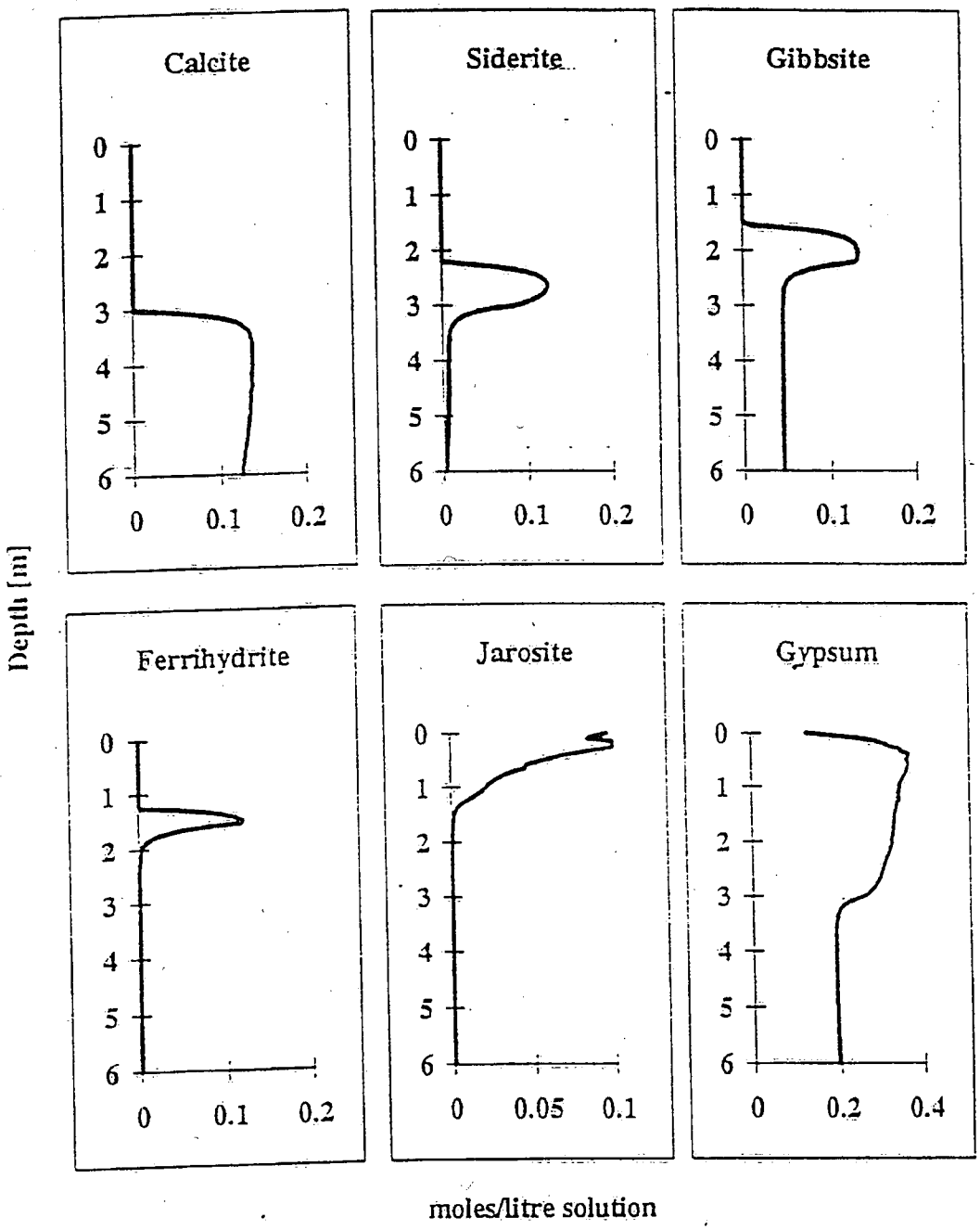

Figure 9. Velocity vectors for 2-D simulations. Units are metres.

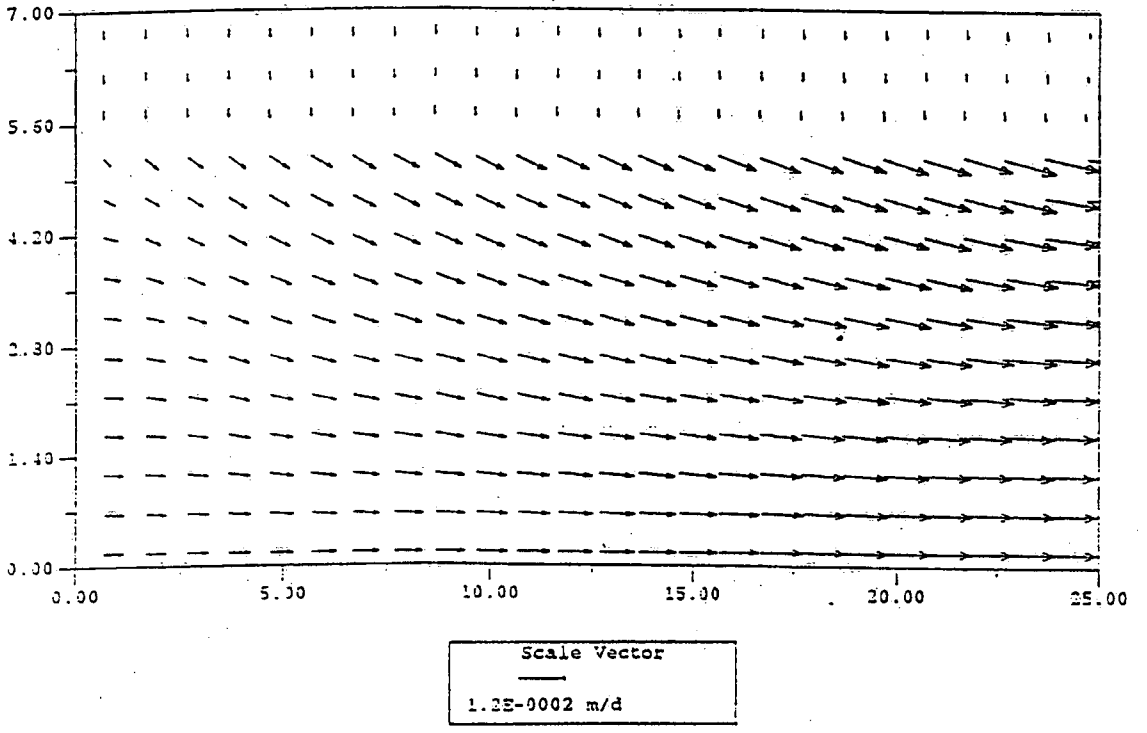

Figure 10. Two dimensional simulation results. Aqueous concentrations and pH. Initial scenario, oxidation time, 10 years.

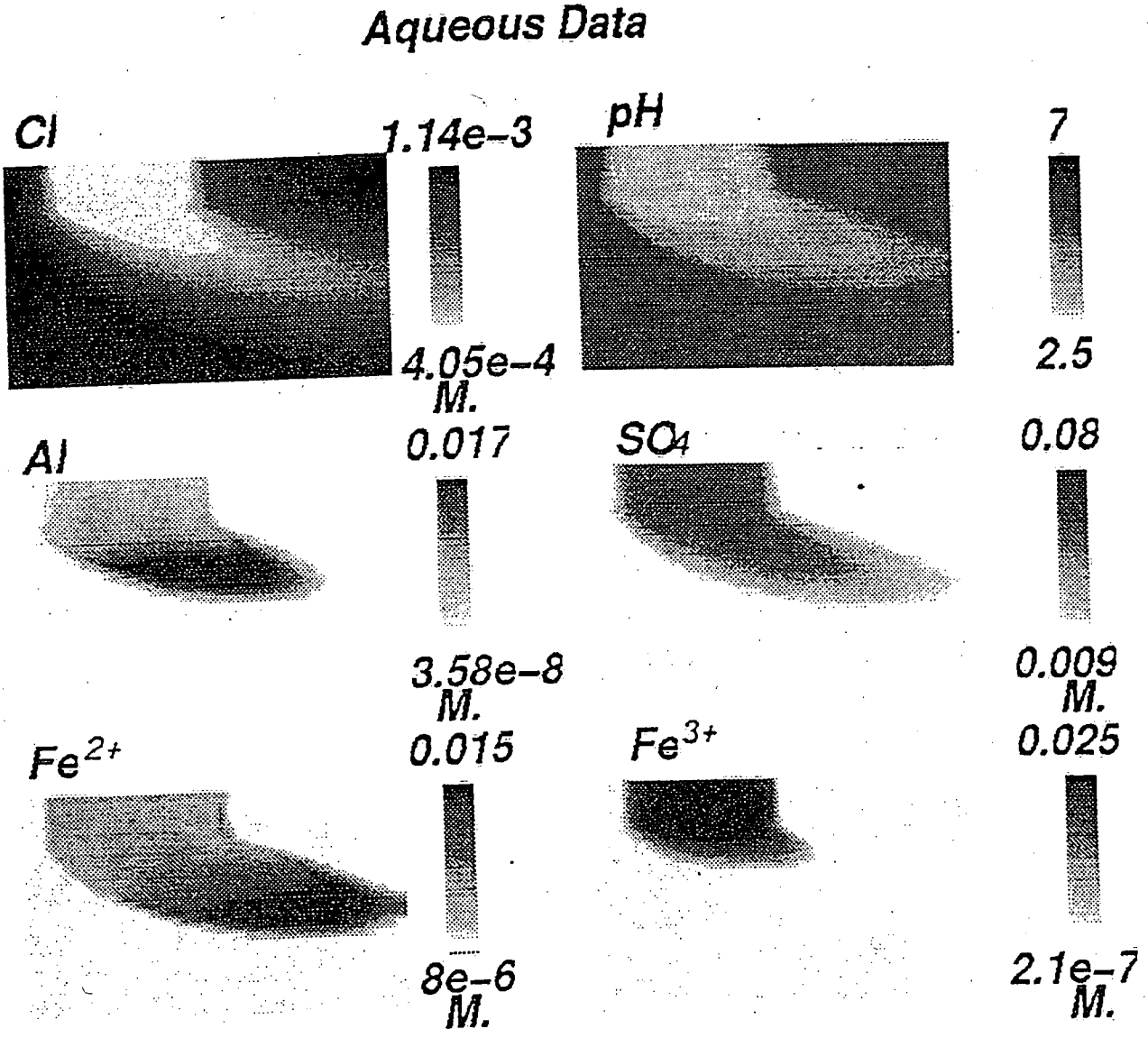

Figure 11. Two dimensional simulation results. Solid concentrations and pe. Initial scenario, oxidation time, 10 years.

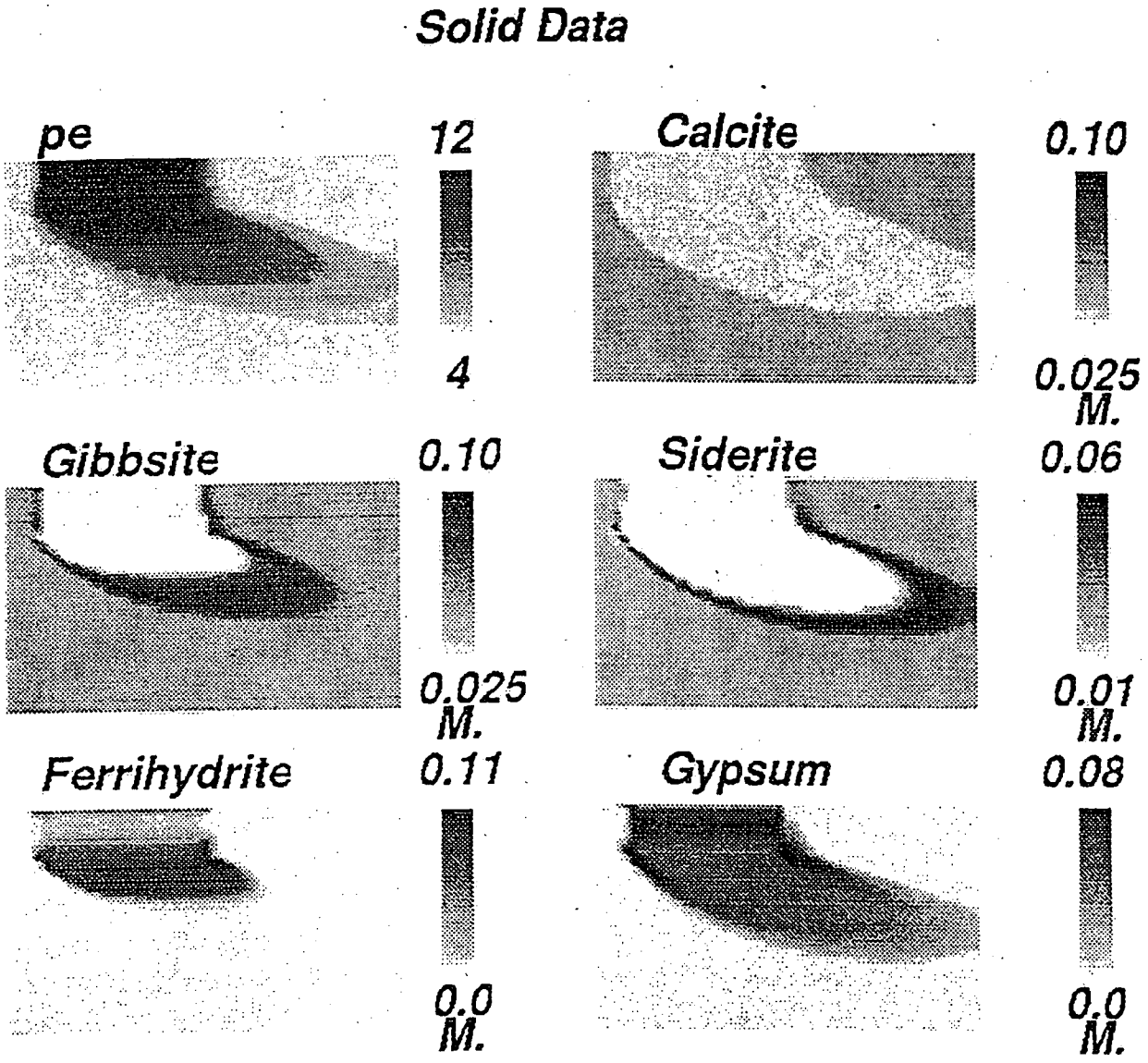

Figure 12. Two dimensional simulation results. Aqueous concentrations and pH. Saturated cover, oxidation time 10 years.

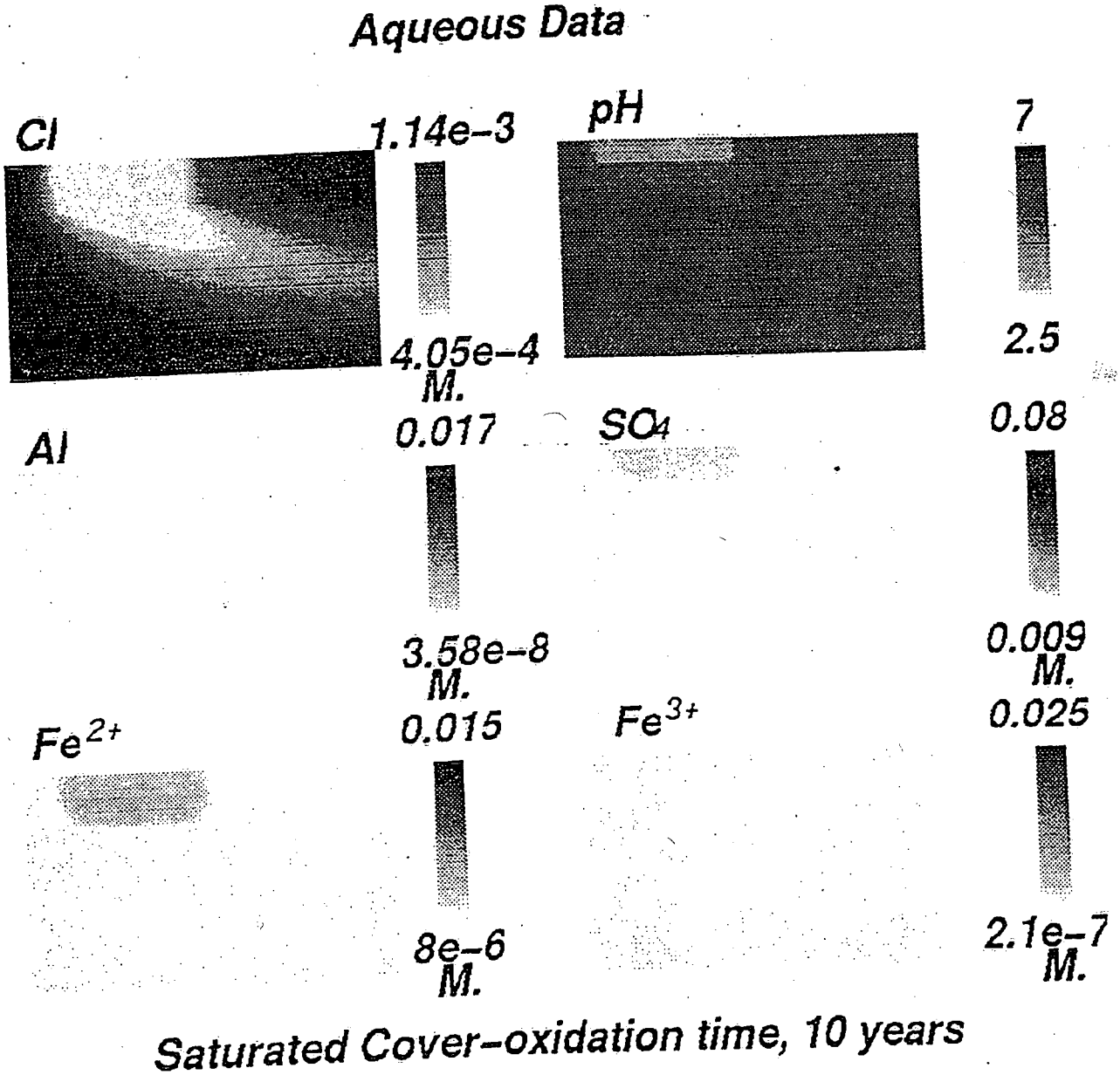

Figure 13. Two dimensional simulation results. Aqueous concentrations and pH. Two wt.% calcite evenly distributed, oxidation time, 10 years.

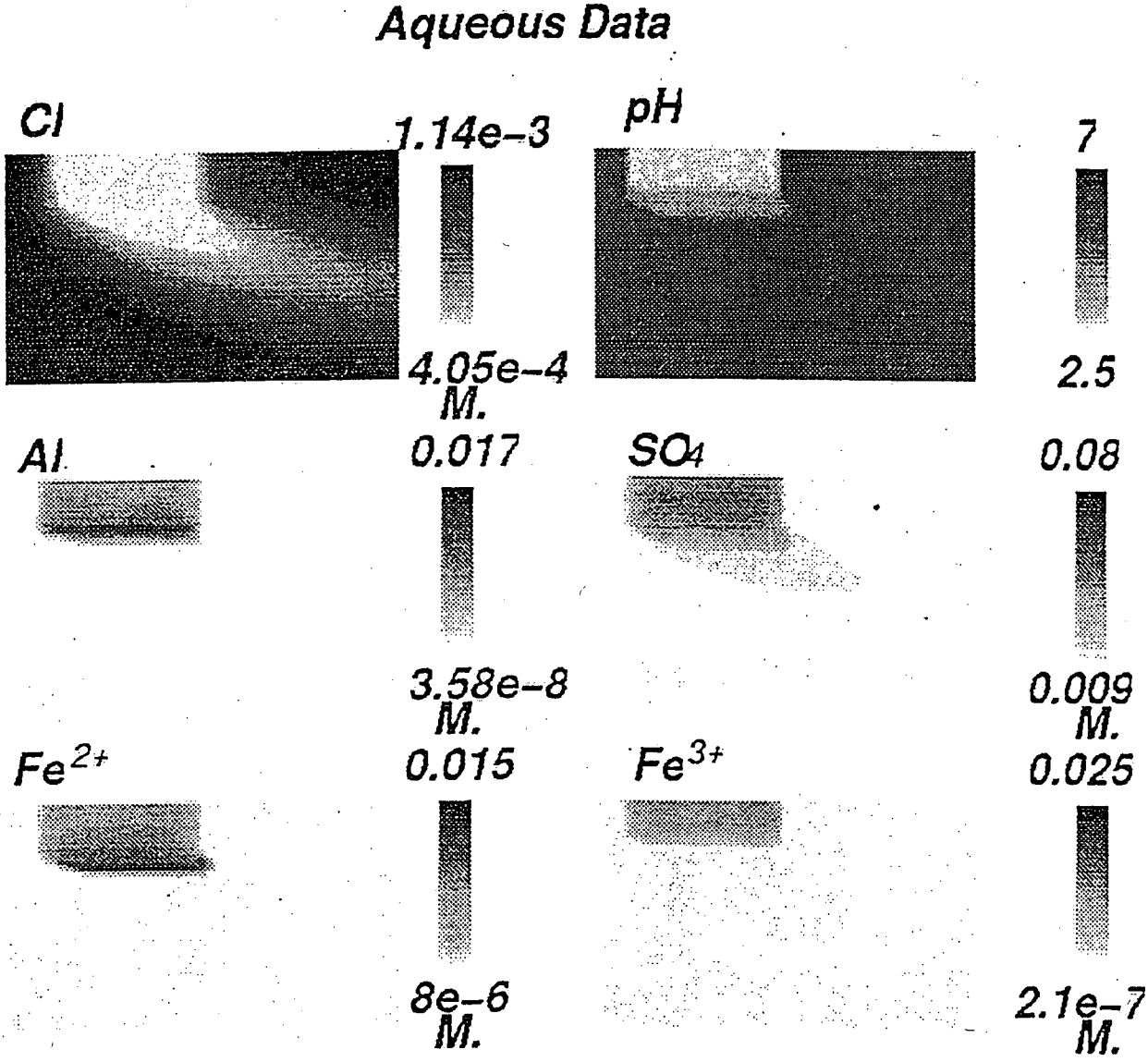

Table 1. Influx chemistry for 1-D simulation.

Aqueous Components	*Concentration moles/litre*
Ca^{2+}	1.25e-2
Mg^{2+}	1.04e-3
K^{+}	9.00e-3
Cl^{-}	1.14e-4
Al^{3+}	1.28e-8
SO_4^{2-}	7.48e-3
Fe^{3+}	2.32e-8
CO_3^{2-}	3.94e-3
H^{+}	4.59e-3
Fe^{2+}	5.36e-5
H_4SiO_4	1.99e-3

Mineral Phase	*Concentration moles/litre*
Calcite	0.070
Lime	0.100
Gibbsite	0.045
Am. Silica	4.69e+1
Siderite	2.00e-2
Ferrihydrite	1.00e-6
Gypsum	0.174
Jarosite	0.0

Table 2. Aqueous background chemistry for 1-D simulation.

Aqueous Components	*Concentration moles/litre*
Ca^{2+}	1.44e-2
Mg^{2+}	2.30e-3
K^{+}	6.00e-3
Cl^{-}	1.14e-3
Al^{3+}	2.59e-8
SO_4^{2-}	3.13e-2
Fe^{3+}	1.48e-7
CO_3^{2-}	3.59e-2
H^{+}	5.47e-2
Fe^{2+}	5.39e-5
H_4SiO_4	1.91e-3

Diffusion Parameter	*Value*
D1	variable [m^2/s]
D2	3.50 E-15 [m^2/s]
Particle Radius	3.0 E-5 [m]
Porosity	variable
Bulk Density	variable [kg/m^3]
% Sulfur	1.61
Depth	6.0 [m]
Time	12.0 [year]
# Nodes	121

Table 3. Solid background chemistry for 1-D simulation.

Table 4. Diffusion parameters for 1-D simulation.

Mineral	*Reaction*	*log K*
Calcite	$Ca^{2+} + CO_3^{2-} \Leftrightarrow CaCO_3$	*8.4789*
Siderite	$Fe^{2+} + CO_3^{2-} \Leftrightarrow FeCO_3$	*10.57*
Gibbsite (c)	$Al^{3+} + 3H_2O \Leftrightarrow Al(OH)_3 + 3H^+$	*-8.11*
Ferrihydrite	$Fe^{3+} + 3H_2O \Leftrightarrow Fe(OH)_3 + 3H^+$	*-4.891*
Jarosite	$K^+ + 3Fe^{3+} + 2SO_4^{2-} + 6H_2O \Leftrightarrow KFe_3(SO_4)_2(OH)_6 + 6H^+$	*9.210*

Table 5. Buffering reactions used in 1-D simulations.

Reaction	ΔH_r^0	log K
$H_2O \Leftrightarrow H^+ + OH^-$	13.345	-13.998
$H_4SiO_4^0 \Leftrightarrow H^+ + H_3SiO_4^-$	8.936	-9.929
$Mg^{2+} + CO_3^{2-} \Leftrightarrow MgCO_3^0$	2.535	2.981
$Mg^{2+} + CO_3^{2-} + H^+ \Leftrightarrow MgHCO_3^+$	-2.775	11.397
$Mg^{2+} + SO_4^{2-} \Leftrightarrow MgSO_4^0$	1.4	2.25
$Ca^{2+} + CO_3^{2-} + H^+ \Leftrightarrow CaHCO_3^+$	-0.869	11.453
$Ca^{2+} + CO_3^{2-} \Leftrightarrow CaCO_3^0$	3.547	3.225
$Ca^{2+} + SO_4^{2-} \Leftrightarrow CaSO_4^0$	1.47	2.309
$K^+ + SO_4^{2-} \Leftrightarrow KSO_4^-$	2.25	0.85
$Al^{3+} + 2H_2O \Leftrightarrow Al(OH)_2^+ + 2H^+$	0.0	-10.1
$Al^{3+} + 4H_2O \Leftrightarrow Al(OH)_4^- + 4H^+$	44.06	-23.0
$Al^{3+} + 3H_2O \Leftrightarrow Al(OH)_3^0 + 3H^+$	0.0	-16.0
$Fe^{2+} + H_2O \Leftrightarrow FeOH^+ + H^+$	13.2	-9.5
$Fe^{2+} + SO_4^{2-} \Leftrightarrow FeSO_4^0$	3.23	2.25
$CO_3^{2-} + H^+ \Leftrightarrow HCO_3^-$	-3.561	10.329
$CO_3^{2-} + 2H^+ \Leftrightarrow H_2CO_3^0$	-5.738	16.681
$Al^{3+} + H_2O \Leftrightarrow AlOH^{2+} + H^+$	11.90	-4.99
$Al^{3+} + SO_4^{2-} \Leftrightarrow AlSO_4^+$	2.15	3.02
$Al^{3+} + 2SO_4^{2-} \Leftrightarrow Al(SO_4)_2^-$	2.84	4.92
$H^+ + SO_4^{2-} \Leftrightarrow HSO_4^-$	4.91	1.987
$Fe^{3+} + H_2O \Leftrightarrow FeOH^{2+} + H^+$	10.399	-2.19
$Fe^{3+} + SO_4^{2-} \Leftrightarrow FeSO_4^+$	3.91	3.92
$Fe^{3+} + 2H_2O \Leftrightarrow Fe(OH)_2^+ + 2H^+$	0.0	-5.67
$Fe^{3+} + 3H_2O \Leftrightarrow Fe(OH)_3^0 + 3H^+$	0.0	-13.6
$Fe^{3+} + 2SO_4^{2-} \Leftrightarrow Fe(SO_4)_2^-$	4.6	5.42
$Fe^{3+} + e^- \Leftrightarrow Fe^{2+}$	-10.0	13.032
$CO_3^{2-} + 2H^+ \Leftrightarrow CO_{2(g)} + H_2O$	-0.53	18.16

Table 6. Species included in 1-D simulation.

Table 7. Influx chemistry for 2-D simulations.

Aqueous Components	*Concentration moles/litre*
Ca^{2+}	1.25e-2
K^{+}	2.56e-4
Cl^{-}	2.80e-4
Al^{3+}	1.28e-7
SO_4^{2-}	7.48e-3
Fe^{3+}	2.32e-8
CO_3^{2-}	3.94e-3
H^{+}	4.59e-3
Fe^{2+}	5.36e-5

Mineral Phase	*Concentration moles/litre*
Calcite	0.05
Gibbsite	5.0e-2
Siderite	2.0e-2
Ferrihydrite	0.5e-3
Gypsum	0.174

Table 9. Solid background chemistry for 2-D simulations

Table 8. Aqueous background chemistry for 2-D simulations.

Aqueous Components	*Concentration moles/litre*
Ca^{2+}	2.64e-2
K^{+}	5.00e-4
Cl^{-}	1.14e-3
Al^{3+}	3.54e-8
SO_4^{2-}	6.19e-3
Fe^{3+}	2.10e-7
CO_3^{2-}	3.30e-2
H^{+}	5.47e-2
Fe^{2+}	9.80e-5

Diffusion Parameter	*Value*
D1 -	variable [m^2/s]
D2	1.0 E-14 [m^2/s]
Particle Radius	7.0 E-5 [m]
Porosity	0.5
Bulk Density	1375 [kg/m^3]
% Sulfur	1.08
Depth	1.5 [m]
Time	10.0 [year]
# Nodes	26

Table 10. Diffusion parameters for 2-D simulations.

APPENDIX

Derivation of the sink term for a single oxidizing particle with a shrinking core (equation 3)

An expression for the diffusional mass flux of oxygen across the outer surface of a reacting particle can be written mathematically as

$$q_s(x,t)=\frac{d(\text{mass}O_2)}{dt}=4\pi R^{*2}Q \qquad (24)$$

where Q is the flux through the particle surface given by Fick's Law

$$Q=-D2\frac{dU_1^*}{dr} \qquad (25)$$

where U_1^* is the concentration of oxygen within the oxidized rim of the particle [kg/m^3].

The mass flux for a single particle will be

$$\frac{d(\text{mass}O_2)}{dt}=-4\pi R^{*2}\ D2\frac{dU_1^*}{dr} \qquad (26)$$

Assuming that the physical transport of oxygen to the reaction site is the rate limiting step, any oxygen reaching the reaction front in a particle will be rapidly consumed relative to the movement of the reaction front and the rate at which oxygen is transported. Thus the oxygen concentration at the reaction front will remain fixed at zero and the following boundary condition can be defined:

$$U_{r_c}^*(x,t)=0 \quad \text{for all } x \text{ and } t.$$

Thus, the concentration of oxygen within the oxidized coating of the particles decreases linearly from the outside of the particle surface to the unreacted core boundary. If equation 26 is integrated from the outer surface to the reaction front, an expression for the rate at which oxygen mass is lost to the particle is derived.

$$\frac{d(\text{mass}O_2)}{dt}\int_{R^*}^{r_c^*}\frac{dr}{r^2}=-4\pi\ D2\int_{U_w^*}^{U_{rc}^*}dU_1^* \qquad (27)$$

Where U^*_w is the concentration of oxygen in the water surrounding the particle [kg/m^3] and $r_c^*(x)$ is the radius of the reaction front within the particle or the radius of the unreacted core [m]. The result is equation 3.

$$q_s(x,t)=\frac{d(\text{mass}\,O_2)}{dt}=4\pi\ D2\left(\frac{R^*r_c^*(x)}{R^*-r_c^*(x)}\right)U_w^*(x,t)$$

Conversion of expressions to dimensionless form

Equations 6 and 9 are written in dimensioned form. The PYROX model was developed with the dimensionless form of the equations and therefore the method of conversion will be outlined. Equation 6 is written as follows:

$$apor(x)\frac{\partial U_A^*(x,t)}{\partial t} = D1(x)\frac{\partial^2 U_A^*(x,t)}{\partial x^2} - \frac{3(1-por(x))D2}{R^{*3}}\left(\frac{R^* r_c^*(x,t)}{R^* - r_c^*(x,t)}\right)U_W^*(x,t)$$

can be made dimensionless with respect to R, x, $r_c(x,t)$, and $U_W(x,t)$ by using the following relationships:

$$U_W(x,t) = \frac{U_W^*(x,t)}{U_0} \quad , \quad r_c(x,t) = \frac{r_c^*(x,t)}{a} \quad , \quad x = \frac{x^*}{L} \quad , \quad R = \frac{R^*}{a} \qquad \textit{(28-31)}$$

The resulting dimensionless form is written as follows (equation 10):

$$apor(x)\frac{\partial U_A(x,t)}{\partial t} = D1(x)\frac{\partial^2 U_A(x,t)}{L^2 \partial x^2} - \frac{3(1-por(x))D2}{a^2}\left(\frac{r_c(x,t)}{1-r_c(x,t)}\right)U_W(x,t)$$

The variables R, $r_c(x,t)$, U_W, and x are now dimensionless with values ranging from 0 to 1.

The same procedure is used to convert equation 9 written as follows:

$$\frac{dr_c^*}{dt} = \frac{D2(1-por)}{\varepsilon\, \rho_s\, r_c^{*2}}\left(\frac{R^* r_c^*(x)}{R^* - r_c^*(x)}\right)U_W^*(x,t)$$

into dimensionless form (equation 11) written as

$$\frac{dr_c}{dt} = \frac{D2(1-por)U_0}{\varepsilon\, \rho_s\, a^2}\left(\frac{1}{r_c(x) - r_c(x)^2}\right)U_W(x,t)$$

GLOSSARY OF TERMS

a	- is the unreacted radius of a particle in the tailings [m].
apor(x)	- is the air-filled porosity of the tailings [m^3/m^3].
alpha(x,t)	- fraction of total pyrite consumed in tailings [kg/kg].
fracsulf(x)	- fraction of sulfur in tailings [kg/kg].

$por(x)$ - is the porosity of the tailings [m^3/m^3].

$q(x,t)$ - is the sink term due to oxygen consumption by the particles in the tailings [kg/m^3s].

$q_s(x,t)$ - is the sink term due to oxygen consumption by a single particle in the tailings [kg/m^3s].

$r_c^*(x)$ - is the radius of the reaction front within the particle or the radius of the unreacted core [m].

w_j - is the linear basis function used in the Galerkin formulation.

$D1(x)$ - is the diffusion coefficient for the porous media [m^2/s].

$D2$ - is the diffusion coefficient for the oxidized rim surrounding the unoxidized core of the particles [m^2/s].

K_{eq} - equilibrium constant for iron [dimensionless].

L - the thickness of the unsaturated zone.[m].

R^* - is the unreacted radius of a particle in the tailings [m].

U_A^* - is the oxygen concentration in the pore space [kg/m^3].

U_W^* - is the concentration of oxygen in the film of water surrounding the particle [kg/m^3].

$XHEN$ - is *1/(Henry's constant for oxygen)* [dimensionless].

ρ_b - bulk density of tailings [kg/m^3].

ε - mass ration of sulfur to O_2 based on stoichiometry of pyrite oxidation (equation 7).

Environment Canada Library, Burlington
3 9055 1017 8244 8

Environment Canada Environnement Canada

Canada

Canada Centre for Inland Waters
P.O. Box 5050
867 Lakeshore Road
Burlington, Ontario
L7R 4A6 Canada

National Hydrology Research Centre
11 Innovation Boulevard
Saskatoon, Saskatchewan
S7N 3H5 Canada

St. Lawrence Centre
105 McGill Street
Montreal, Quebec
H2Y 2E7 Canada

Place Vincent Massey
351 St. Joseph Boulevard
Gatineau, Quebec
K1A 0H3 Canada

Centre canadien des eaux intérieures
Case postale 5050
867, chemin Lakeshore
Burlington (Ontario)
L7R 4A6 Canada

Centre national de recherche en hydrologie
11, boul. Innovation
Saskatoon (Saskatchewan)
S7N 3H5 Canada

Centre Saint-Laurent
105, rue McGill
Montréal (Québec)
H2Y 2E7 Canada

Place Vincent-Massey
351 boul. St-Joseph
Gatineau (Québec)
K1A 0H3 Canada